Aus der

Poliklinik für Zahnärztliche Prothetik

Klinikum der Ludwig-Maximilians-Universität München

Chemische und mechanische Eigenschaften 3D-gedruckter Harze zur Herstellung von Prothesenbasen

Dissertation

zum Erwerb des Doktorgrades der Zahnmedizin

an der Medizinischen Fakultät der

Ludwig-Maximilians-Universität München

vorgelegt von

Veronika Geiger

aus

München

Jahr 2024

Mit Genehmigung der Medizinischen Fakultät
der Ludwig-Maximilians-Universität München

Erstes Gutachten:	Prof. Dr. Bogna Stawarczyk
Zweites Gutachten:	PD Dr. Marcel Reymus
Drittes Gutachten:	PD Dr. Nikolaus Thierfelder

Mitbetreuung durch den promovierten Mitarbeiter:	_____
Dekan:	Prof. Dr. med. Thomas Gudermann

Tag der mündlichen Prüfung: 22.07.2024

Affidavit

LMU LUDWIG-MAXIMILIANS-UNIVERSITÄT MÜNCHEN

Dekanat Medizinische Fakultät
Promotionsbüro

Eidesstattliche Versicherung

Geiger, Veronika

Name, Vorname

Ich erkläre hiermit an Eides statt, dass ich die vorliegende Dissertation mit dem Thema

Chemische und mechanische Eigenschaften
3D-gedruckter Harze zur Herstellung von Prothesenbasen

selbständig verfasst, mich außer der angegebenen keiner weiteren Hilfsmittel bedient und alle Erkenntnisse, die aus dem Schrifttum ganz oder annähernd übernommen sind, als solche kenntlich gemacht und nach ihrer Herkunft unter Bezeichnung der Fundstelle einzeln nachgewiesen habe.

Ich erkläre des Weiteren, dass die hier vorgelegte Dissertation nicht in gleicher oder in ähnlicher Form bei einer anderen Stelle zur Erlangung eines akademischen Grades eingereicht wurde.

Leonberg, 23.07.2024
Ort, Datum

Veronika Geiger
Unterschrift Veronika Geiger

Inhaltsverzeichnis

Abkürzungsverzeichnis

CAD – Computer-aided design

CAM – Computer-aided manufacturing

PMMA – Polymethylmethacrylat

SLA – Stereolithographie

DLP – Digital light processing

FDP – Fixed dental prothesis

RDP – Removable dental prothesis

ISO – International Organization for Standardization

K_{IC} – Bruchzähigkeit

FS – Biegefestigkeit

Publikationsliste

Greil V, Mayinger F, Reymus M, Stawarczyk B. Water sorption, water solubility, degree of conversion, elastic indentation modulus, edge chipping resistance and flexural strength of 3D-printed denture base resins. J Mech Behav Biomed Mater 2023; 137: 105565 (doi: 10.1016/j.jmbbm.2022.105565)

IF 2023: 4.042

Geiger V, Mayinger F, Hoffmann M, Reymus M, Stawarczyk B. Fracture toughness, work of fracture, flexural strength and elastic modulus of 3D-printed denture base resins in two measurement environments after artificial aging. J Mech Behav Biomed Mater 2023; 150: 106234 (doi: 10.1016/j.jmbbm.2023.106234)

IF 2023: 4.042

Beitrag zu der Promotion

Der eigene Beitrag zu der Promotion sowie zu den beiden Publikationen „Water sorption, water solubility, degree of conversion, elastic indentation modulus, edge chipping resistance and flexural strength of 3D-printed denture base resins" und „Fracture toughness, work of fracture, flexural strength and elastic modulus of 3D-printed denture base resins in two measurement environments after artificial aging " kann der folgenden Tabelle entnommen werden.

	Veronika Geiger	**Prof. Dr. Bogna Stawarczyk**	**Co-Autoren**
Literaturrecherche	80%	10%	10%
Projektidee	-	60%	40%
Vorversuche	30%	10%	60%
Einarbeitung in die Prüfkörperherstellung	30%	10%	60%
Einarbeitung in die Ramanspektroskopie	30%	-	70%
Entwicklung einer neuen Prüfmethode	85%	5%	10%
Verfassen einer Arbeitsanweisung zur Herstellung von Bruchzähigkeitskörpern nach ISO-Norm	100%	-	-
Deutschsprachiger Übersichtsartikel zum Thema „Update 3-D-Druck – wo stehen wir und wo wollen wir hin?" (Quintessenz Zahntechnik)	70%	10%	20%
Deutschsprachiger Übersichtsartikel zum Thema „Werkstoffwissenschaftliche Aspekte von 3-D-Druckharzen für herausnehmbare Versorgungen." (Quintessenz Zahntechnik)	90%	5%	5%
Verfassen eines Online-Beitrags „Dentaler 3D-Druck – ein Überblick" (European Association of Dental Technology)	90%	5%	5%
Präsentation der Promotion im Rahmen eines Forschungspreises (VOCO Dental Challenge)	90%	3%	7%

„Water sorption, water solubility, degree of conversion, elastic indentation modulus, edge chipping resistance and flexural strength of 3D-printed denture base resins"			
Konzepterstellung	-	60%	40%
Auswahl und Beschaffung der Prüfmaterialien	-	10%	90%
Supervision der Untersuchungen	-	10%	90%
Prüfkörperherstellung und Alterung	90%	-	10%
Datenerhebung	90%	-	10%
Deskriptive statistische Analyse	70%	20%	10%
Explorative statistische Analyse	10%	90%	-
Tabellen und Abbildungen	90%	5%	5%
Manuskripterstellung	60%	10%	30%
Durchsicht und Überarbeitung des Manuskripts	-	20%	80%
„Fracture toughness, work of fracture, flexural strength and elastic modulus of 3D-printed denture base resins in two measurement environments after artificial aging "			
Konzepterstellung	-	60%	40%
Auswahl und Beschaffung der Prüfmaterialien	-	10%	90%
Supervision der Untersuchungen	-	10%	90%
Prüfkörperherstellung und Alterung	90%	-	10%
Datenerhebung	100%	-	-
Deskriptive statistische Analyse	80%	10%	10%
Explorative statistische Analyse	20%	80%	-
Tabellen und Abbildungen	90%	5%	5%
Manuskripterstellung	60%	10%	30%
Durchsicht und Überarbeitung des Manuskripts	-	10%	90%

1. Einleitung

Die zunehmende Digitalisierung der Zahnmedizin führt weg von manuellen Fertigungsmethoden hin zu digitalen CAD/CAM-Fertigungsverfahren, welche bereits Einzug in viele Dentallabore erhalten hat [1]. Die Anfänge der CAD/CAM-Technologie liegen in den 1980er Jahren und hat die Vielseitigkeit, Genauigkeit und Zeit-Kosteneffizienz zahnmedizinischer Arbeiten verbessert [2]. Lange Zeit konnte der CAM-Prozess mit der subtraktiven Fertigung gleichgesetzt werden, bei der ein Objekt durch Fräsen oder Schleifen aus einem vorpolymerisierten PMMA-Rohling gefertigt wird [3]. Bei der Herstellung musste allerdings ein hoher Verschleiß der Fräswerkzeuge sowie ein Materialverlust von bis zu 90% in Kauf genommen werden [4]. Im Gegensatz dazu, werden Objekte bei der additiven Fertigung (3D-Druck) schichtweise aufgebaut, was eine hohe Präzision, die Realisierung komplexer Dimensionen, z.B. die Einarbeitung von Innenhohlräumen, und eine Verringerung des Materialabfalls auf 40% ermöglicht [5–7].

Die in der Zahnmedizin am weitesten verbreiteten 3D-Drucktechnologien sind SLA (Stereolithographie) und DLP (Digital Light Processing) [8]. Dabei werden lichtempfindliche Materialien auf PMMA-Basis in 50-200 µm dicken Schichten mit Hilfe einer UV-Lichtquelle polymerisiert, um die gewünschte Form des Objekts zu erzeugen [9,10,7]. Während die additive Herstellung von provisorischem und definitivem festsitzendem Zahnersatz (FDP) wie Inlays, Onlays und Kronen bereits seit mehreren Jahren untersucht wird, ist die additive Herstellung von herausnehmbarem Zahnersatz (RDP) erst kürzlich in den Fokus von in-vitro- und klinischen Untersuchungen gerückt [11–13].

Für den langfristigen Einsatz der Prothesenbasismaterialien am Patienten müssen die Materialien eine hohe orale Stabilität aufweisen. Das bedeutet unter anderem eine geringe Wasserabsorption und Wasserlöslichkeit, eine hohe Umsetzungsrate um biologische Effekte durch Restmonomere zu vermeiden und ausreichend hohe mechanische Eigenschaften, um den auftretenden Kaukräften standzuhalten [6,14]. Aufgrund der Polarität der Acrylketten in den Kunststoffe neigen sie durch molekulare Wechselwirkungen und das Eindringen von Feuchtigkeit in Mikroporen dazu, in feuchter Umgebung über einen längeren Zeitraum Wasser zu absorbieren [15,16].

Um eine hohe Biokompatibilität zu gewährleisten ist es außerdem wichtig, die Menge der unpolymerisierten Monomere so gering wie möglich zu halten, um Reizungen und Schäden an der Mundschleimhaut des Patienten zu verhindern [17]. Während der Funktion sind Prothesen aufgrund der Kaukräfte hohen Belastungen ausgesetzt, insbesondere bei zahnlosen Patienten, da hier das Rückkopplungssystem des parodontalen Ligaments fehlt, was zu Rissen und Frakturen der Prothesenbasen führen kann [18].

Um die intraorale Umgebung unter standardisierten Laborbedingungen zu reproduzieren und um die Auswirkungen der auftretenden Temperaturschwankungen in der oralen Umgebung auf die gedruckten Restaurationen zu untersuchen, kann ein Thermolastwechsler eingesetzt werden [19,20]. Die kritischen Materialeigenschaften, die in der ISO-Norm (International Organization for Standardization) für Materialien auf Polymerbasis [21] festgelegt sind, werden zur Vorhersage der klinischen Leistung der untersuchten Materialien verwendet [3].

2. Zielsetzung

In den zwei dieser Dissertation zugrundeliegenden international veröffentlichten Publikationen wurden die chemischen und mechanischen Eigenschaften 3D-gedruckter Prothesenkunststoffe in-vitro untersucht. Ziel war es den Einfluss der Wahl des Materials, der Alterung und der Prüfumgebung auf die Materialeigenschaften 3D-gedruckter Prothesenbasiskunststoffe zu messen und die Ergebnisse zu interpretieren.

Die Herstellung der Prüfkörper und die Ermittlung der Materialeigenschaften wurden nach den Vorgaben der ISO-Norm für Prothesenkunststoffe durchgeführt und die Ergebnisse wurden mit den in der Norm festgelegten Grenzwerten verglichen.

Um die Materialeigenschaften der intraoralen Umgebung unter standardisierten Laborbedingungen möglichst kliniknah zu simulieren, wurden zusätzlich unterschiedliche künstliche Alterungsmethoden angewendet.

3. Material und Methoden

Als 3D-Druck Harze wurden NextDent Denture 3D+ (NextDent), Fotodent Denture (Dreve ProDiMed), Freeprint Denture (DETAX) und V-Print dentbase (VOCO) verwendet, welche für herausnehmbaren Zahnersatz zugelassen sind. Ivotion Base (Ivoclar Vivadent) wurde als fräsbares und PalaXpress (Kulzer) als autopolymerisierendes Vergleichsmaterial in der ersten Untersuchung verwendet.

Untersuchung I

Bei der ersten Untersuchung wurden insgesamt 540 Prüfköper aus vier 3D-druckbaren, einem fräsbaren und einem autopolymerisierenden Prothesenkunststoff in drei unterschiedlichen Geometrien hergestellt. Für die Messung der Wasseraufnahme und Wasserlöslichkeit wurden Scheiben mit den Maßen 50±0.1 × 0.5±0.05 mm, für die Umsetzungsrate, das elastische Eindringungsmodul und die Kantenstabilität rechteckige Blöcke mit den Maßen 5 × 10 × 25 mm und für die Biegefestigkeit rechteckige Stäbchen mit den Maßen 3.3±0.2 mm × 10.0±0.2 mm × 64.0 mm angefertigt. Das Post-Processing, wie die Reinigung in Isopropanol, sowie die Nachbelichtung erfolgten nach Herstellerangaben. Die Prüfkörper wurden unter Wasserkühlung auf die endgültigen Abmessungen poliert und die Maße mit einer digitalen Mikrometerschraube mit einer Genauigkeit von ±4 µm überprüft.

Die Prüfkörper jedes Materials wurden in zwei Alterungsgruppen aufgeteilt:

1. Lagerung in 37 °C temperiertem Wasser für 24 h
2. Lagerung in 37 °C temperiertem Wasser für 24 h und 5.000x Thermozyklen (5/55°C mit einer Verweilzeit von 30 s)

Zur Bestimmung der Wasseraufnahme und der Wasserlöslichkeit wurden die Prüfkörper nach der Alterung in einem Exsikkator mit Kieselgel aufbewahrt und in einem Ofen bei 37±1 °C für 23±1 h gelagert. Die Scheiben wurden dann in einen zweiten Exsikkator (23±2 °C) mit Kieselgel für 60±10 min überführt und mit einer analytischen Waage mit einer Genauigkeit von 0,2 mg gewogen. Der Trocknungszyklus wurde wiederholt, bis sich eine konstante Masse eingestellt hat. Zu diesem Zeitpunkt wurde das Volumen der Prüfkörper bestimmt. Anschließend wurden die Prüfkörper in Wasser (37±1 °C) gelagert, und die Gewichtszunahme nach 7d±2h gemessen. Im letzten Schritt wurden die Prüfkörper nach der gleichen Trocknungsmethode rekonditioniert, bis sie eine konstante Endmasse erreichten.

Für die Bestimmung der Umsetzungsrate wurden Raman-Streuungen der unpolymerisierten und polymerisierten Materialien mit einem konfokalen Raman-Spektrophotometer erfasst. Die Messungen wurden mit einem Diodenlaser bei einer Wellenlänge von 785 nm und einer spektralen Auflösung von 1 cm^{-1} durch ein Mikroskopobjektiv (50×) durchgeführt. Die resultierenden Spektren wurden analysiert und die Bandenhöhen bei den Peaks 1.640 cm^{-1} und 1.610 cm^{-1} ermittelt.
Die Kantenstabilität und das elastische Eindringungsmodul wurden mit einer Martens-Härte-Maschine und die Biegefestigkeit mit einer Universalprüfmaschine gemessen.

Untersuchung II

Im zweiten Teil der Untersuchungen wurden insgesamt 480 rechteckige Prüfkörper in zwei unterschiedlichen Geometrien (für Bruchzähigkeit K_{IC}: 4.0±0.2 mm × 8.0±0.2 mm × 39.0 mm; für FS: 3.3±0.2 mm × 10.0±0.2 mm × 64.0 mm) aus vier verschiedenen 3D-Druck Prothesenkunststoffen im DLP-Druckverfahren hergestellt. Das Post-Processing, wie die Reinigung in Isopropanol, sowie die Nachbelichtung erfolgten nach Herstellerangaben. Die Prüfkörper wurden unter Wasserkühlung auf die endgültigen Abmessungen poliert und die Maße mit einer digitalen Mikrometerschraube mit einer Genauigkeit von ±4 µm überprüft.
Die Prüfkörper jedes Materials wurden in drei Alterungsgruppen aufgeteilt:

1. Wassergelagert: Lagerung in 37°C temperiertem Wasser für 50 h (FS-Proben) oder 7 d (K_{IC}-Proben)
2. Hydrothermal-gealtert: Lagerung in 37°C temperiertem Wasser für 50 h/7 d und hydrothermale Alterung für 20 min (0,2 MPa, 134°C)
3. Thermolastwechsler-gealtert: Lagerung in 37°C temperiertem Wasser für 50 h/7 d und 10.000x thermische Zyklen (5/55°C mit einer Verweilzeit von 30 s)

Jede Untergruppe wurde in zwei Messumgebungen getestet:

a) Luft bei 23°C (die Prüfkörper wurden vor der Messung 60 Minuten lang in 23°C temperiertem Wasser konditioniert)
b) Wasser bei 37°C (nach Erreichen eines Temperaturgleichgewichts)

Bruchzähigkeit und Biegefestigkeit wurden in einer Universalprüfmaschine gemessen, wobei die Brucharbeit und das Elastizitätsmodul aus den Last-Durchbiegungskurven berechnet wurden und eine fraktographische Analyse der Biegefestigkeitsprüfkörper durchgeführt wurde.

Statistische Auswertung

Bei der statistischen Auswertung beider Untersuchungen wurde die Abweichung von der Normalverteilung der Daten mit dem Kolmogorov-Smirnov-Test überprüft und die globale univariate Varianzanalyse mit partiellem Eta-Quadrat angewandt, um die Effektstärke der getesteten Parameter zu bestimmen. Um die Unterschiede zwischen den untersuchten Gruppen zu ermitteln, wurden die nicht-parametrischen Tests Kruskal-Wallis-H und Mann-Whitney-U angewendet. Die Spearman-Korrelation wurde berechnet, um die Assoziationen zwischen den getesteten Parametern zu untersuchen. Bei der zweiten Untersuchung wurde zudem die Zwei-Parameter-Weibull-Analyse angewendet, um die Zuverlässigkeit der beobachteten Werte zu abzuschätzen.

4. Ergebnisse

Die vier 3D-gedruckten Prothesenkunststoffe zeigten untereinander große Unterschiede in den Materialeigenschaften. Dabei hatte die Wahl des Materials den größten Einfluss auf die gemessene Wasseraufnahme, Wasserlöslichkeit, das elastische Eindringungsmodul, die Umsetzungsrate und Biegefestigkeit. Die 3D-gedruckten Harze wiesen im Vergleich zu den Kontrollgruppen, dem gefrästen und dem autopolymerisierten Harz, höhere mechanische Eigenschaften aber auch höhere Wasseraufnahme- und Wasserlöslichkeitswerte auf. Bis auf die Kantenstabilität und die Umsetzungsrate, wurden alle untersuchten Parameter durch die künstliche Alterung negativ beeinflusst, wobei die 3D-gedruckten Materialien eine höhere Anfälligkeit für Alterung zeigten.

Hydrothermale Alterung (134 °C, 0,2 MPa, 20 min) und Alterung im Thermolastwechsler (10.000×, 5/55°C) führten zu einer Verringerung der Bruchzähigkeit, Brucharbeit, Biegefestigkeit und dem E-Modul. Dabei zeigten die hydrothermal gealterten Gruppen niedrigere Werte als die im Thermolastwechsler gealterten Prüfkörper. Die Messungen an der Luft (23°C) führten zu höheren Biegefestigkeitswerten und einem spröderen Bruchverhalten als die Messungen, welche im Wasser (37°C) durchgeführt wurden, wobei die Messumgebung keinen klaren Einfluss auf die Bruchzähigkeit zeigte. Rund 30% der getesteten Fotodent Denture Biegefestigkeitsprüfkörper brachen während der Messungen nicht, da bis zum Erreichen der eingestellten Grenzwerte der Prüfmaschine nur eine Durchbiegung, aber kein Bruch stattfand. Die Prüfungen, bei denen die Prüfkörper nicht brachen, wurden von der statistischen Analyse ausgenommen.

5. Diskussion

Da alle vier additiv hergestellten Prothesenbasiskunststoffe mit denselben Parametern (Belichtungszeit, Schichtstärke, Temperatur) gedruckt wurden, unterschieden sich die Prüfgruppen nur anhand der Zusammensetzung des Harzes und der angewandten Nachbearbeitungsmethode. Da die genaue Zusammensetzung vom Hersteller nicht bekannt gegeben wird, ist es schwierig, die Unterschiede in den mechanischen Eigenschaften der untersuchten Materialien auf die einzelnen Komponenten zurückzuführen. Mehrere Untersuchungen haben jedoch gezeigt, dass eine effiziente Nachhärtung zu adäquaten mechanischen Eigenschaften führt, indem sie den Umwandlungsgrad erhöht [22]. Die Wirksamkeit des Nachhärtungsverfahrens ist eng mit den verwendeten Wellenlängen der Polymerisationsgeräte verbunden. So kann es sein, dass die Wellenlängen der emittierten Strahlung eines Nachpolymeristationsgerätes nicht oder nur gering mit dem Absorptionsspektrum des Photoinitiators der Harze überlappen. Der in allen vier Materialien enthaltene Photoinitiator, Trimethylbenzoyl-Diphenyl-Phosphinoxid (TPO), weist ein Absorptionsmaximum bei etwa 380 nm auf [23,24]. Diese Wellenlänge wird von den Strahlungsspektren der beiden, in diesen Untersuchungen verwendeten Polymerisationsgeräten (UV-Lichtbox, Otoflash) abgedeckt. Dennoch können die Unterschiede der Herstellerangaben in Belichtungsintensität und Belichtungsdauer zu unterschiedlichen Umsetzungsraten und somit zu unterschiedlichen chemischen und mechanischen Eigenschaften der 3D-gedruckten Prothesenkunststoffen geführt haben.

Die künstliche Alterung simuliert die intraorale Umgebung der prothetischen Versorgungen im Patienten unter standardisierten Laborbedingungen. Dabei kann die Anfälligkeit der Materialien für Alterung die Langzeitstabilität in der Mundhöhle beeinträchtigen. Das Eindringen von Wasser in die Kunststoffmatrix während des Alterungsprozesses kann zu einer Erweichung des Materials führen, sowie die Bindung zwischen den verschiedenen Druckschichten beeinträchtigen und somit zu einem erhöhten Auftreten von Delaminationen zwischen diesen Schichten führen [25]. Die fraktographischen Analysen zeigten, dass die gealterten Gruppen bei der Biegefestigkeitsprüfung in weniger Bruchstücke zerbrachen, was auf ein weniger sprödes Verhalten der Kunststoffe hindeutet. Um Unebenheiten auf der Oberfläche der Prüfkörper, die den Ursprung des Bruchs darstellen können zu verringern, können optimierte Polierprotokolle oder eine Versiegelung der Oberfläche durch Coating sinnvoll sein.

Die größere Wirkung der hydrothermalen Alterung auf die Biegefestigkeit lässt sich durch die Wärmeempfindlichkeit der Hauptbestandteile der Prothesenbasisharze erklären. Das Erhitzen im Autoklaven auf 134 °C kann die Polymerstruktur der Kunststoffe teilweise auflösen und in Kombination mit der Anwendung von Druck zu einer Beeinträchtigung der Integrität der Prüfkörper und folglich zu einer Verringerung ihrer mechanischen Eigenschaften führen [26].

Die Prüfung in verschiedenen Messumgebungen ergab keine eindeutigen Trends für die Bruchzähigkeit, bei der Biegefestigkeit ergaben die Messungen in Luft höhere Werte als in Wasser. Möglicherweise wurde bei der Prüfung der Prüfkörper in Wasser Feuchtigkeit durch bereits vorhandene Löcher, Risse und Spalten zwischen den Druckschichten in das Material aufgenommen. Die Porositäten sind auf den additiven Fertigungsprozess zurückzuführend und wurden durch die Alterung noch verstärkt, wodurch die mechanischen Eigenschaften der Kunststoffe verringert wurden [27]. Die hohe Wasseraufnahme und Wasserlöslichkeit der 3D-gedruckten Materialien und eine Verringerung des Elastizitätsmoduls deutet darauf hin, dass Messungen in Wasser zu einem elastischeren Verhalten der Kunststoffe führen. Die in Luft gemessenen hohen Biegefestigkeiten können daher die Vorhersagen für die klinische Situation verzerren, die durch ihre feuchte Umgebung bei Körpertemperatur definiert ist. Um aussagekräftigere Prognosen zur Integrität eines Materials in-situ zu ermöglichen, sollten in-vitro-Messungen daher in Wasser bei 37 °C durchgeführt werden. Die Tatsache, dass ein großer Teil der Prüfkörper während der Messungen nicht frakturierte, sondern bis zum Erreichen der maximalen Auslenkung verformt wurde, stellt die in den ISO-Normen festgelegten Messmethoden in Frage. Eine frühere Untersuchung hat bereits die Begründung der Grenzwerte in der ISO-Norm kritisiert [28] und die Notwendigkeit einer überarbeiteten Definition der Messaufbauten und der erforderlichen Grenzwerte unterstrichen, die die elastischen Eigenschaften der für die additive Fertigung von Prothesenbasismaterialien verwendeten 3D-Druckharze berücksichtigen.

6. Zusammenfassung

Ziel der vorliegenden Dissertation war es im ersten Teil, den Einfluss der Wahl des Prothesenbasismaterials und der Alterung auf die chemischen und mechanischen Eigenschaften zu untersuchen. Im zweiten Teil war das Ziel der Untersuchung den Einfluss der künstlichen Alterung und der Messumgebung auf die mechanischen Eigenschaften von vier 3D-gedruckten Prothesenbasismaterialien zu untersuchen.

Die Untersuchungen zeigten, dass die 3D-gedruckten Harze im Vergleich zu den Kontrollgruppen höhere mechanische Eigenschaften, allerdings auch eine höhere Wasseraufnahme sowie Wasserlöslichkeit aufwiesen. Die künstliche Alterung beeinflusste alle gemessenen Materialparameter, wobei hydrothermales Altern zu niedrigeren Bruchzähigkeits- und Biegefestigkeitswerten geführt hat als Thermocycle-Alterung. 3D-gedruckte Kunststoffe zeigten zudem eine größere Anfälligkeit für Alterung als der autopolymerisierende und fräsbare Kunststoff. Messungen in Luft (23 °C) führten zu höheren Biegefestigkeitswerten und einem spröderen Bruchverhalten als Messungen in Wasser (37 °C).

7. Abstract (English)

In the first investigation of this dissertation the influence of the choice of the material and aging on the material properties of denture base resins was determined. The second investigation examined the mechanical properties of four 3D-printed denture base materials after artificial aging and in two measurement environments.

The investigations reported that the 3D-printed materials showed higher mechanical properties compared to the control groups, but also a higher water sorption and water solubility. Artificial aging influenced all measured material parameters, with hydrothermal aging leading to lower fracture toughness and flexural strength values than thermocycle aging. The 3D-printed denture materials also showed a higher susceptibility to aging than the autopolymerized and milled control groups. Measurements in air (23°C) resulted in higher flexural strength values and more brittle fracture behavior than measurements in water (37°C).

Veröffentlichung I

journal of the mechanical behavior of biomedical materials 137 (2023) 105565

Contents lists available at ScienceDirect

Journal of the Mechanical Behavior of Biomedical Materials

journal homepage: www.elsevier.com/locate/jmbbm

Water sorption, water solubility, degree of conversion, elastic indentation modulus, edge chipping resistance and flexural strength of 3D-printed denture base resins

Veronika Greil [a,*,1], Felicitas Mayinger [a,1], Marcel Reymus [b], Bogna Stawarczyk [a]

[a] Department of Prosthetic Dentistry, Dental School, University Hospital, LMU Munich, Goethestraße 70, 80336, Munich, Germany
[b] Department of Conservative Dentistry and Periodontology, Dental School, University Hospital, LMU Munich, Goethestraße 70, 80336, Munich, Germany

ARTICLE INFO

Keywords:
Denture base resin materials
3D-printing
Chemical properties
Mechanical properties

ABSTRACT

Objectives: To investigate the water sorption (w_{sp}), water solubility (w_{sl}), degree of conversion (*DC*), elastic indentation modulus (E_{IT}), edge chipping resistance (*ECR*) and flexural strength (*FS*) of 3D-printed, milled and conventionally polymerized denture base resin materials.
Methods: Specimens (N = 540) were 3D-printed (NextDent Denture 3D+ (DEN), Fotodent Denture (FOT), Freeprint Denture (FRE), V-Print dentbase (VPR)), cut (Ivotion Base (IVO)) and molded (PalaXpress (PAL)) in three geometries. W_{sp}, w_{sl}, *DC*, E_{IT}, *ECR* and *FS* were tested initially (24 h, 37 °C, H20) and after additional aging (5000 thermal cycles, 5/55 °C). Data were analyzed with Kolmogorov-Smirnov, univariate ANOVA, Kruskal-Wallis, Mann-Whitney *U* test and Spearman's correlation ($p < 0.05$)
Results: Most 3D-printed denture base resins showed higher w_{sp} (25.31–37.94 μg/mm^3) and w_{sl} (0.08–8.27 μg/mm^3), but also higher E_{IT} (3.11–4.09 GPa) and *FS* (60.81–99.57N/mm^2) values than the control groups. DEN and VPR showed high *DC* (89.36–93.53%), E_{IT} (3.77–4.09 GPa) and *FS* (79.65–99.57N/mm^2), while FOT showed low w_{sp} (25.31–27.35 μg/mm^3) and w_{sl} (1.01–3.87 μg/mm^3) values. In all materials, the examined parameters were affected by aging.
Significance: Although 3D-printed denture base resins showed promising results with regard to the observed *DC* and *FS*, only FOT and FRE surpassed the threshold values defined by the ISO norms.

1. Introduction

With the increasing digitalization in dentistry, the production of dental restorations has also been moving from traditional manual to digital CAD/CAM manufacturing processes that have now become commonplace in many dental laboratories (Dawood et al., 2015). For a long time, the CAM process could be equated with subtractive manufacturing, where an object is formed out of a prepolymerized PMMA blank using milling or grinding (Oliveira Limírio et al., 2021). However, to fabricate dental restorations, a high wear of the milling tools and a material loss of up to 90% had to be accepted (Strub et al., 2006). In contrast, using additive manufacturing, objects with more complex geometries can be produced and the loss of material can be reduced to 40% (Alharbi et al., 2017). The most widespread 3D printing technologies in dentistry are SLA (stereolithography) and DLP (Digital Light Processing) (Kessler et al., 2020). Here, photosensitive resin-based materials are polymerized in 50–200 μm thick layers by using an UV light source to create the desired shape of the object (Tian et al., 2021; Whitley et al., 2017; Bilgin et al., 2016). Typical application areas of 3D printing in dentistry are the production of models and splints for implantology, orthodontics and endodontics, and the production of fixed and removable dental prostheses (Tian et al., 2021).

Polymethyl methacrylate (PMMA) is the most used material for the manufacturing of denture bases. While previously processed by injection molding or milling, it can now also be processed using a 3D printer. For its long-term use as a denture base material, the printed bases must show a high oral stability, which, inter alia, means a low water absorption and water solubility, a high degree of conversion to avoid biological effects from residual monomers and high mechanical properties to withstand masticatory forces (Aati et al., 2022; Zafar, 2020). Due to the polarity of

* Corresponding author. Department of Prosthetic Dentistry, University Hospital, LMU Munich, Goethestrasse 70, 80336, Munich, Germany.
E-mail address: veronika.greil@med.uni-muenchen.de (V. Greil).
[1] Veronika Greil and Felicitas Mayinger contributed equally to this work.

https://doi.org/10.1016/j.jmbbm.2022.105565
Received 19 September 2022; Received in revised form 5 November 2022; Accepted 7 November 2022
Available online 11 November 2022

acrylic resins, they tend to absorb water over a longer period of time in humid environments through the penetration of liquids into micro-voids or particular molecular interactions (Gad et al., 2022; Perea-Lowery et al., 2021). Sorption (w_{sp}) and solubility (w_{sl}) are important indicators for assessing the durability of denture resins, as the interaction of water and the polymer chains leads to internal stresses because of swelling, chemical degradation and the solution of residual monomers (Gad et al., 2022; Perea-Lowery et al., 2021). To ensure a high biocompatibility, it is furthermore important to keep the amount of residual monomers as low as possible. Measuring the degree of conversion (*DC*) of the resin provides information about the amount of unpolymerized monomer, which can cause irritation and damage to the oral mucosa of the patient (Bartoloni et al., 2000). During function, dentures are subjected to high stresses due to the masticatory forces, especially in edentulous patients that lack the feedback system of the periodontal ligament, which can lead to cracks and fractures of the denture bases (Alhareb et al., 2017). Determining the mechanical properties of a material, e.g., the elastic indentation modulus (E_{IT}) which is calculated from the unloading curve of the indentation and correlates positively with the modulus of elasticity, the edge chipping resistance (*ECR*) and the flexural strength (*FS*), help to predict the resistance of the printed object to deformation and fracture and to determine the integrity of the removable protheses. To examine the effects of the occurring temperature fluctuations in the oral environment on the printed restorations, thermocycling can be used (Gale and Darvell, 1999; Li et al., 2021). In this investigation, 5000 cycles (5/55 °C) were employed, which is supposed to correspond to a residence time of 6 months in the oral cavity (Gad et al., 2022).

The aim of this investigation was to examine the influence of the denture base resin material, namely four 3D-printed, one milled and one conventional autopolymerizing resin, and aging on the chemical and mechanical properties. The tested null hypotheses stated that neither the choice of denture base material nor aging showed an impact on w_{sp}, w_{sl}, *DC*, E_{IT}, *ECR* and *FS* and that no correlations existed between the different parameters.

2. Materials and methods

The chemical and mechanical properties of four 3D-printed, one milled and one conventional autopolymerizing denture base resin were examined (Fig. 1).

The 3D-print materials (NextDent Denture 3D+ (abbreviated with: DEN, Lot No: WY475N01), NextDent, Soesterberg, Netherlands; Fotodent Denture (FOT, Lot No: 010086X1), Dreve ProDiMed, Unna, Germany; Freeprint Denture (FRE, Lot No: 241,203), DETAX, Ettlingen, Germany; V-Print dentbase (VPR, Lot No: 2122339), VOCO, Cuxhaven, Germany) were additively manufactured with a layer height of 50 µm and a vertical orientation of the specimens on the printing platform using a DLP printer (Rapidshape D20 II, Rapid Shape, Heimsheim, Germany; Table 1). The denture base blank (Ivotion Base (IVO, Lot No: YB3JR1, YB22PS), Ivoclar Vivadent, Schaan, Liechtenstein) was cut using a cutting machine (Secotom 50, Struers, Ballerup, Denmark) and the autopolymerizate (PalaXpress (PAL, Lot No: K010229, 010,513), Kulzer, Hanau, Germany) was manufactured using molds.

The specimens were polished using a series of silicon carbide papers from P500 up to P1200 under water-cooling (Abramin, Struers) and cleaned in an ultrasonic bath (L&R Transistor/Ultrasonic T-14, L&R Ultrasonics, New Jersey, USA) with distilled water. Finals dimensions were verified with a digital micrometer screw with an accuracy of ±4 µm (IP65, Mitutoyo, Kawasaki, Japan).

A total of 540 specimens were prepared in three geometries (N = 540, n = 180/geometry). For specimen geometry (1) - w_{sp}/w_{sl}, (2) - *DC*/E_{IT}/*ECR*, and (3) - *FS*, 30 specimens of each material were manufactured (n = 30/material) and divided into two different aging groups (n = 15/aging):

1) storage in 37 °C tempered water (HERAcell 150, Thermo Fisher Scientific, Waltham, USA) for 24 h, hereafter abbreviated with initial,
2) storage in 37 °C tempered water for 24 h and 5,000x thermal cycles (5/55 °C with a dwell time of 30 s; Thermocycler THE-1100, SD Mechatronik, Feldkirchen-Westerham, Germany), abbreviated with aged.

2.1. Water sorption and solubility

For w_{sp} and w_{sl} measurements, 180 disc-shaped specimens (50 ± 0.1 × 0.5 ± 0.05 mm) were manufactured according to DIN EN ISO 20795–1 (DIN EN ISO, 20795, 2079). After aging, the specimens were kept inside a desiccator containing freshly dried silica gel and stored in an oven (Modell 100–800, Memmert, Schwabach, Germany) at 37 ± 1 °C for 23 ± 1 h. The discs were then transferred to a second desiccator (23 ± 2 °C) with freshly dried silica gel for 60 ± 10 min. Thereafter, the specimens were weighed using an analytical balance (NewClassic MF, Mettler-Toledo, Greifensee, Switzerland) with an accuracy of 0.2 mg. The described drying cycle was repeated until a constant mass (m_1) was reached. At that time, the volume (*V*) was measured by taking the mean diameter and thickness of each specimen. Afterwards, the specimens

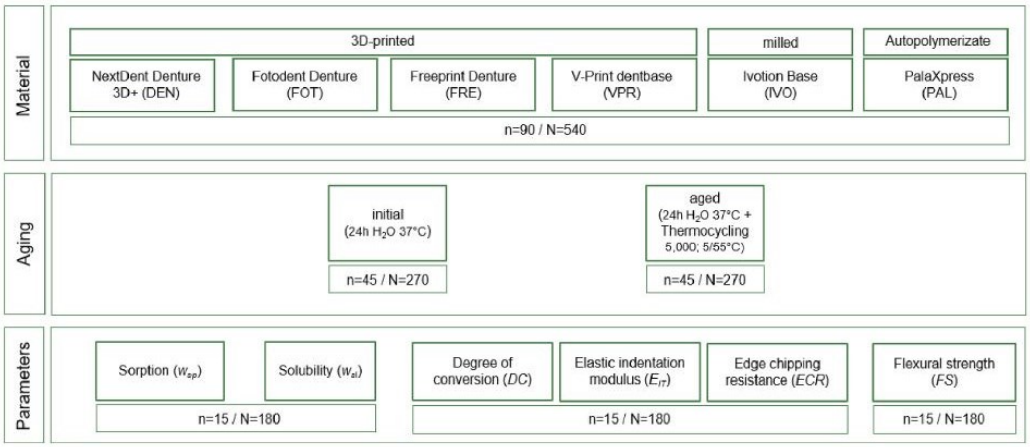

Fig. 1. Study design.

Table 1
Examined 3D-printed materials and respective post-curing devices.

3D-printed resin	Composition	Post-curing device	Duration/ Flashes	Wavelength	Peaks	Intensity
Denture 3D+ (NextDent)	- Ethoxylated bisphenol A dimethacrylate (>75%) - 7,7,9(7,9,9)- trimethyl-4,13-dioxo-3,14-dioxa-5,12-diazahexadecane-1,16-diyl bismethacrylate (10–20%) - 2-hydroxyethyl methacrylate (5–10%) - silicon dioxide (1–5%) - Diphenyl (2,4,6-trimethylbenzoyl) phosphine Oxide (1–5%) - Titanium dioxide (<0,1%)	UV-Lightbox[a]	30 min	315–550 nm	360 + 435 nm	six 1.7 W UV lamps + six 2.3 W UV lamps
Fotodent Denture (Dreve)	- Neopentyl glycol(PO)2 diacrylate (25–50%) - Aliphatic urethane dimethacrylate (25–50%) - Aliphatic urethane trimethacrylate (10–25%) - Diphenyl (2,4,6-trimethylbenzoyl) phosphine Oxide (<2,5%) - Color pigment concentrate (<2,5%)	Flashlight lamp[b](under nitrogen atmosphere)	2 × 4000	280–580 nm	480 + 530 nm	1.4 W/cm^2 per flash
Freeprint Denture (Detax)	- Isopropylidenediphenol Peg-2 dimethacrylate (35–60%) - 7,7,9(7,9,9)- trimethyl-4,13-dioxo-3,14-dioxa-5,12-diazahexadecane-1,16-diyl bismethacrylate (30–35%) - 2-hydroxyethyl methacrylate (1–5%) - Diphenyl (2,4,6-trimethylbenzoyl) phosphine Oxide (1–5%) - Hydroxypropyl methacrylate (1–5%) - 1,6-hexandiol dimethacrylate (1–5%) - Phenylbis (2,4,6-trimethylbenzoyl) phosphine oxide (<1%)	Flashlight lamp[b](under nitrogen atmosphere)	2 × 2000	280–580 nm	480 + 530 nm	1.4 W/cm^2 per flash
V-Print dentbase (VOCO)	- Aliphatic urethane dimethacrylate (50–100%) - Ethoxylated bisphenol A dimethacrylate (25–50%) - triethylene glycol dimethacrylate (5–10%) - Diphenyl (2,4,6-trimethylbenzoyl) phosphine Oxide (<2,5%)	UV-Lightbox[a]	30 min	315–550 nm	360 + 435 nm	six 1.7 W UV lamps + six 2.3 W UV lamps

[a] UV-Lightbox: LC-3DPrint Box (NextDent).
[b] Flashlight-lamp: Otoflash G171 (NK-Optik GmbH).

were stored in water (37 ± 1 °C) and the weight gain was recorded after 7d±2h (m_2). As a final step, the specimens were reconditioned following the same drying method until they attained a final constant mass (m_3).

$$w_{sp} = \frac{m_2 - m_3}{V}$$

$$w_{sl} = \frac{m_1 - m_3}{V}$$

with m_1: mass of the conditioned specimens (μg), m_2 mass after water storage (μg), m_3 mass of the reconditioned specimens (μg) and V: volume (mm^3)

2.2. Degree of conversion

The *DC* of the 3D-printed denture base materials was measured using rectangular specimens (5 × 10 × 25 mm). The Raman scatterings of the unpolymerized and polymerized materials were acquired by using a confocal Raman spectrophotometer (InViaQontor, Renishaw, New Mills, UK). A total of 15 measurements were performed for each material to determine an average value for the unpolymerized Raman scattering $R_{unpolymerized}$. The polymerized specimens were tested to determine R_{cured}. The measurements were performed by a diode laser at a wavelength of 785 nm and a spectral resolution of 1 cm^{-1} through a microscope objective (50 ×). For each measurement, ten accumulations at a power of 100% and an irradiation time of 10 s were conducted. The resulting spectra were analysed with the software WiRE 4.2 (Renishaw) and the band heights at peaks 1640 cm^{-1} (absorbance intensity ratio of methacrylate Cfx2C) and 1610 cm^{-1} (absorbance intensity ration of aromatic Cfx2C) were detected.

$$DC = 100 * \left[1 - \frac{\left(\frac{A_{1640}}{A_{1610}}\right) polymerised}{\left(\frac{A_{1640}}{A_{1610}}\right) unpolymerised} \right]$$

with A_{1640}: band height at 1640 cm^{-1} and A_{1610}: band height at 1610 cm^{-1}

2.3. Elastic indentation modulus

For the E_{IT} measurements, the Vickers diamond indenter pyramid (α = 136°) of a Martens hardness machine (ZHU 0.2; Zwick Roell, Ulm, Germany) was lowered vertically and pressed into the rectangular specimens' surface with a load of 9.8 N for 10 s.

The E_{IT} values were calculated (testX-pert V12.3 Master software, ZwickRoell) according to ISO 14577–1 (DIN EN ISO 14577, 1457):

$$E_{IT} = \left(1 - \nu_S^2\right) \left(\frac{\sqrt[2]{A_p(h_c)}}{\sqrt{\pi}\, S} - \frac{\left(1 - \nu_i^2\right)}{E_i} \right)^{-1}$$

with E_{IT}: elastic modulus of indenter (kN/mm^2), $A_p(hc)$: projected contact area under load (mm^2), ν_s: Poisson's ratio of the specimen and ν_i: Poisson's ratio of the indenter, S: contact stiffness evaluated from the force removal curve.

2.4. Edge chipping resistance

To determine the *ECR* with a Martens hardness machine (ZHU 0.2), the rectangular specimens were fixed with a double-sided adhesive tape and the tip of the Vickers diamond indenter (α = 136°) was positioned 0.3 mm from the edge of the specimens. The distance between the edge of the specimens and the Vickers diamond was checked by using the in-built optical microscope unit (magnification × 5, camera resolution: 1.4

megapixel) and kept constant at 0.3 mm for all measurements.

The pyramid was lowered at a speed of 10 mm/min until chipping occurred and the measurement end was defined as a 10% drop of the actual force (Fig. 2).

The determined maximum force value was used to calculate the *ECR* and was considered as chipping force F_{max}. Edge chipping resistance was calculated according to the technical standard CEN/TS 843–9:2010 (DIN CEN, 2010):

$$ECR = \frac{F_{max}}{0.3mm}$$

with F_{max}: maximum force (*N*)

2.5. Flexural strength

The bar specimens for 3-point *FS* measurement (3.3 ± 0.2 mm × 10.0 ± 0.2 mm × 64.0 mm) were centrally placed in the specific specimen holder. *FS* was measured in 37 °C tempered water at a crosshead speed of 5 mm/min in a displacement-controlled mode until fracture occurred or the maximum testing distance of 10 mm was reached (Fig. 3).

3-point *FS* was calculated:

$$\sigma = \frac{3Fl}{2bh^2}$$

with *F*: fracture load (*N*); *l*: bearing range (*mm*); b_t: specimen thickness (*mm*); h_t: specimen height (*mm*)

2.6. Statistical analyses

Descriptive statistics were calculated, and the distribution of the data was examined with the Kolmogorov-Smirnov test. Univariate ANOVA with partial eta squared (η_p^2) was used to analyze the impact of the different variables on w_{sp}, w_{sl}, *DC*, E_{IT}, *ECR* and *FS*. The significant differences between the material and artificial aging groups were determined by using the Kruskal-Wallis and Mann-Whitney *U* test. Spearman's correlation was calculated between w_{sp}, w_{sl}, *DC*, E_{IT}, *ECR* and *FS*. *P*-values below 0.05 were viewed as statistically significant (IBM Statistics SPSS 26.0, IBM, Amonk, USA).

3. Results

A deviation from the normal distribution was indicated for 29 of the 64 investigated groups; results were analyzed non-parametrically.

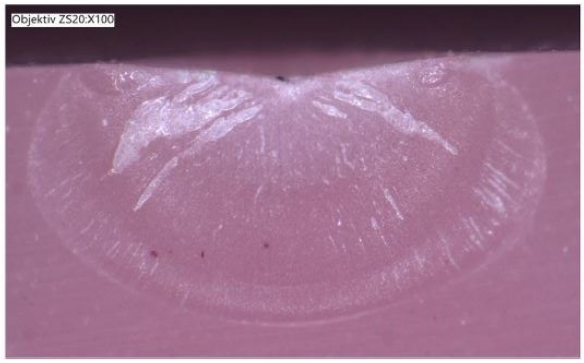

Fig. 2. A light microscopic image (Keyence VHX-970F, Keyence, Osaka, Japan) of a chipping surface, showing the indentation area and the radial direction of crack propagation.

Fig. 3. Set-up for the 3-point *FS* measurement in 37 °C tempered water.

3.1. Water sorption and solubility

The choice of the different materials showed the highest influence on the w_{sp} values ($\eta_p^2 = 0.930$, $p < 0.001$), followed by the aging method ($\eta_p^2 = 0.133$, $p < 0.001$). Initially, VPR showed the highest w_{sp} values, followed by DEN, FRE, FOT and PAL ($p < 0.001$–0.019) (Table 2). After aging, VPR and DEN showed the highest w_{sp} values, followed by FRE, FOT and PAL ($p < 0.001$–0.101). IVO showed the lowest w_{sp} ($p < 0.001$) in both aging levels. DEN, FOT, PAL and IVO showed higher w_{sp} values after aging than initially ($p < 0.001$). VPR showed higher values in the initial group ($p = 0.010$). In FRE, no difference was observed between the two aging levels ($p = 0.983$).

The aging level showed a higher influence on the w_{sl} ($\eta_p^2 = 0.965$, $p < 0.001$) than the different materials ($\eta_p^2 = 0.951$, $p < 0.001$). Initially, VPR showed the highest w_{sl} values followed by FRE, DEN/FOT, and IVO, while PAL showed the lowest values ($p < 0.001$–0.178). After aging, FOT showed the highest w_{sl} values, followed by DEN/FRE and PAL/IVO ($p < 0.001$–0.272). VPR showed the lowest values ($p < 0.001$–0.272). For PAL, no difference was observed between the two aging levels ($p = 0.290$). All other materials showed higher values initially than after aging ($p < 0.001$).

3.2. Degree of conversion

As the Raman spectra of the monomer of the conventionally manufactured resin showed no detectable peaks and as the unpolymerized resin of the milled blank wasn't available, the DC of IVO and PAL could not be determined. The choice of the different materials showed the highest influence on the *DC* ($\eta_p^2 = 0.922$, $p < 0.001$), followed by the aging level ($\eta_p^2 = 0.086$, $p = 0.002$). Initially, DEN showed the highest *DC* values, followed by VPR and FRE, while FOT showed the lowest values ($p < 0.001$) (Fig. 4). Within the aged groups, DEN and VPR

Table 2
Descriptive statistics (mean, standard deviation (SD) and 95% confidence intervals (CI)) for w_{sp} (μg/mm^3), w_{sl} (μg/mm^3), E_{IT} (GPa) and FS (N/mm^2) of the different groups.

	DEN		FOT		FRE		VPR		IVO		PAL	
	Mean ± SD	95% CI	Mean ± SD	95% CI	Mean ± SD	95% CI	Mean ± SD	95% CI	Mean ± SD	95% CI	Mean ± SD	95% CI
Initial												
w_{sp}	32.66 ± 1.25^{e,A}	31.8; 33.4	25.31 ± 2.80^{a,c,A}	23.6; 26.9	29.48 ± 2.08^{d,A}	28.2; 30.7	37.94 ± 1.55^{f,B}	36.9; 38.8	22.55 ± 0.77^{a,A}	22.0; 23.0	24.87 ± 1.16^{a,b,A}	24.1; 25.6
w_{sl}	3.72 ± 0.25^{c,B}	3.4; 3.9	3.87 ± 0.49^{a,c,B}	3.4; 4.2	6.80 ± 0.56^{d,B}	6.3; 7.2	8.27 ± 0.67^{e,B}	7.7; 8.7	1.12 ± 0.12^{b,B}	0.9; 1.2	0.28 ± 0.15^{a,a,A}	0.1; 0.4
E_{IT}	3.93 ± 0.14^{ac,B}	3.7; 4.1	3.15 ± 0.05^{a,a,A}	3.0; 3.2	3.69 ± 0.43^{ac,A}	3.3; 4.0	4.09 ± 0.14^{d,A}	3.9; 4.2	3.33 ± 0.12^{b,B}	3.1; 3.4	3.78 ± 0.33^{ac,A}	3.4; 4.0
FS	90.44 ± 4.10^{ac,B}	88.0; 92.8	69.75 ± 3.65^{b,B}	67.6; 71.8	96.13 ± 8.41^{d,B}	91.3; 100.8	99.57 ± 4.89^{d,B}	96.7; 102.3	71.50 ± 5.79^{b,B}	68.1; 74.8	66.32 ± 4.58^{a,A}	63.6; 68.9
Aged												
w_{sp}	36.12 ± 0.64^{ae,B}	35.6; 36.5	27.35 ± 0.75 ^{c,B}	26.8; 27.8	29.35 ± 1.69^{d,A}	28.3; 30.3	36.65 ± 0.88^{e,A}	36.0; 37.2	23.43 ± 0.97^{aa,B}	22.7; 24.0	26.42 ± 0.92 ^{b,B}	25.8; 27.0
w_{sl}	0.86 ± 0.20^{ac,A}	0.6; 1.0	1.01 ± 0.44^{a,d,A}	0.6; 1.3	0.74 ± 0.20^{c,A}	0.5; 0.9	0.08 ± 0.06^{a,A}	0.1; 0.2	0.15 ± 0.11^{ab,A}	0.1; 0.3	0.22 ± 0.13^{b,A}	0.1; 0.3
E_{IT}	3.77 ± 0.24^{ab,A}	3.5; 4.0	3.11 ± 0.07^{a,a,A}	2.9; 3.2	3.69 ± 0.34^{ab,A}	3.3; 3.9	4.03 ± 0.09^{a,c,A}	3.8; 4.1	2.95 ± 0.46^{aa,A}	2.5; 3.3	3.61 ± 0.45^{ab,A}	3.2; 3.9
FS	79.65 ± 3.92^{c,A}	77.3; 81.9	60.81 ± 3.47^{a,A}	58.7; 62.8	89.57 ± 14.62^{ad,A}	81.3; 97.7	89.26 ± 6.29^{d,A}	85.6; 92.8	59.18 ± 6.09^{a,A}	55.7,62.6	69.22 ± 3.63^{ab,A}	67.1; 71.3

^{a,b,c,d,e,f} indicate significant differences between the materials within one aging level.
^{A,B} indicate significant differences between the aging levels within one material.
CI Confidence interval.
SD Standard deviation.
^{a} Deviation from the normal distribution.

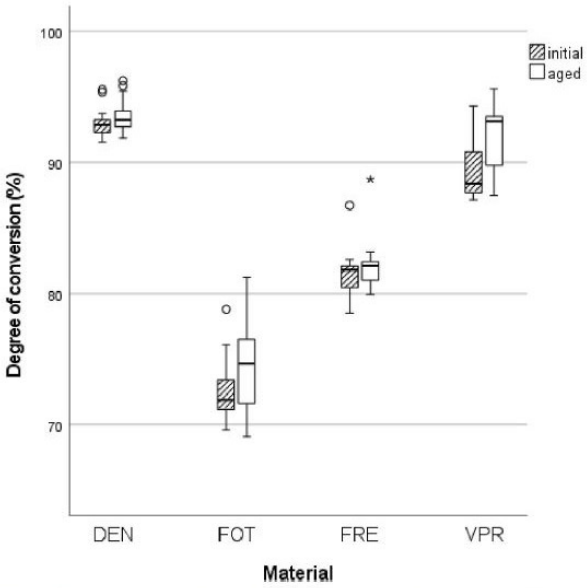

Fig. 4. Degree of conversion of the four tested 3D-print materials (Median, 25%-Quartile, 75%-Quartile, standard deviation, outliers ° and extreme outliers *).

showed the highest values, followed by FRE and FOT ($p < 0.001$–0.191). For DEN, FOT and FRE, no difference was observed between the two aging levels ($p = 0.165$–0.206). VPR showed higher values after aging than initially ($p = 0.014$).

3.3. Elastic indentation modulus

The choice of the different materials showed the highest influence on the E_{IT} ($\eta_p^2 = 0.619$, $p < 0.001$), followed by the aging method ($\eta_p^2 = 0.057$, $p = 0.002$). Initially, VPR showed the highest E_{IT} values, followed by DEN/FRE/PAL, IVO and FOT ($p < 0.001$–0.898). After aging, VPR showed the highest values, followed by DEN/FRE/PAL and FOT/IVO ($p < 0.001$–0.730). For FOT, FRE, VPR and PAL, no difference was observed between the two aging levels ($p = 0.130$–0.265). DEN and IVO showed higher values initially than after aging ($p < 0.001$).

3.4. Edge chipping resistance

In contrast to the choice of material ($p = 0.882$), the aging level showed an influence on the *ECR* ($p = 0.047$). For DEN, FOT and VPR, no difference was observed between the two aging levels ($p = 0.663$–0.983). FRE showed higher values initially than after aging ($p = 0.007$) (Fig. 5). The ECR for IVO and PAL could not be determined, as no chipping occurred.

3.5. Flexural strength

The choice of the different materials showed the highest influence on the *FS* values ($\eta_p^2 = 0.802$, $p < 0.001$), followed by the aging level ($\eta_p^2 = 0.270$, $p < 0.001$). Initially, FRE and VPR showed the highest *FS* values, followed by DEN and FOT/IVO, while PAL showed the lowest values ($p < 0.001$–0.576). After aging, FRE and VPR showed the highest values, followed by DEN and PAL, while FOT and IVO showed the lowest values ($p < 0.001$–0.694). For PAL, no difference was observed between the two aging levels ($p = 0.054$). All other materials showed higher values initially than after aging ($p < 0.001$–0.015).

W_{sp} correlated positively with w_{sl} ($R = 0.272$, $p < 0.001$), *DC* ($R = 0.795$, $p < 0.001$), E_{IT} ($R = 0.607$, $p < 0.001$) and *FS* ($R = 0.703$, $p < 0.001$). W_{sl} showed a positive correlation with *FS* ($R = 0.450$, $p < 0.001$). *DC* showed a positive correlation with E_{IT} ($R = 0.631$, $p < 0.001$) and *FS* ($R = 0.420$, $p < 0.001$). E_{IT} correlated positively with *FS* ($R = 0.647$, $p < 0.001$).

4. Discussion

The aim of this investigation was to examine the chemical and mechanical properties of four 3D-printed denture base resins in comparison with one milled and one conventional autopolymerizing denture base resin. The tested null hypotheses that neither the choice of denture base

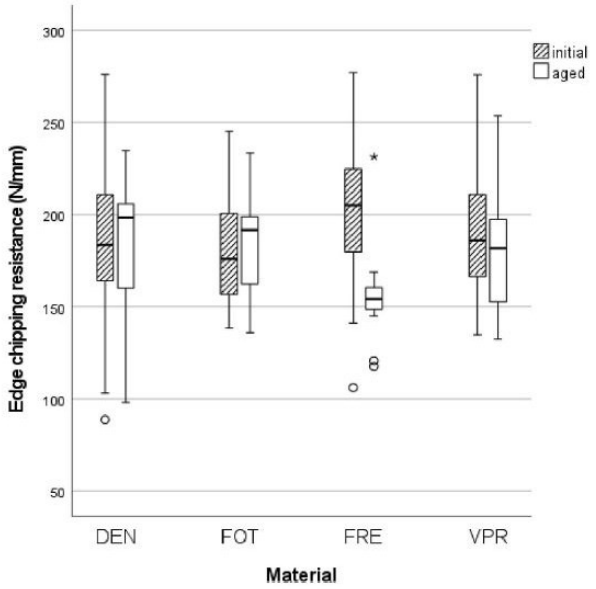

Fig. 5. Edge chipping resistance of the four tested 3D-print materials (Median, 25%-Quartile, 75%-Quartile, standard deviation, outliers ° and extreme outliers *).

material nor aging showed an impact on w_{sp}, w_{sl}, *DC*, E_{IT}, *ECR* and *FS* and that no correlations existed between the different parameters were rejected.

Regardless of the aging level, the 3D-printed materials showed higher w_{sp} and w_{sl} values than the two control groups. Apart from the w_{sp} values obtained by VPR and DEN and the w_{sl} initially reported for VPR, the 3D-printed materials surpassed the threshold values defined for w_{sp} and w_{sl} by the ISO norm (w_{sp}: 32 μg/mm^3 and w_{sl}: 8 μg/mm^3). In a clinical situation, VPR and DEN may thus absorb an excessive amount of water, which would increase the volume of the denture and lead to a decrease in the fit and hold of the prosthesis. These findings agree with previous investigations that have shown that 3D-printed resins had a higher w_{sp} and higher w_{sl} than conventionally autopolymerizing resins and that there is a positive association, although weak, between w_{sp} and w_{sl} (Gad et al., 2022; Perea-Lowery et al., 2021; Berli et al., 2020). This may be caused by water that is absorbed between the printing layers diffusing into interpolymeric spaces, resulting in an increased w_{sl}. In addition, 3D printed resins may have a higher proportion of residual monomers, which can be dissolved during storage in water (Gad et al., 2022). A decreased layer thickness during printing or the subsequent pursuit of specific polishing protocols or surface sealing with coatings may improve the surface quality of 3D-printed objects and reduce the high water absorption that has been observed for these materials (Kraemer Fernandez et al., 2020). Since it is not yet apparent how coated objects behave in a long-time use, e.g. in terms of abrasion resistance or tendency to discoloration additional investigations are warranted, especially in regard to the w_{sp} and higher w_{sl} of coated materials. In contrast to a previous investigation, which showed no difference in w_{sp} and w_{sl} between a CAD/CAM PMMA-disc and conventional PMMA, PAL showed higher w_{sp} in both aging levels, while IVO presented higher initial w_{sl} values (Hada et al., 2021). While the findings regarding w_{sp} acknowledge the potential advantages of an industrial manufacturing of CAD/CAM discs (Hada et al., 2021), the higher w_{sl} observed for IVO narrows the benefit of this manufacturing process and calls for further investigations. Among the 3D-printed resins, VPR showed the highest w_{sp} and w_{sl} in the initially tested groups and together with DEN also the highest w_{sp} after aging. This is a puzzling finding, as VPR and DEN showed a high *DC*. It can thus be assumed that the two materials possess a low monomer content and should therefore, in theory, show low w_{sp} and w_{sl} values. A potential explanation may be that the 3D-printed objects were, however, overcured during post-polymerization. This overcuring has led to a higher DC and a lower amount of residual monomer trapped in the internal network which interferes with water molecules, that made the 3D-printed objects susceptible to w_{sp} and w_{sl} (Aati et al., 2022). Further investigations are necessary to investigate the cause for these findings more closely. In accordance with a previous investigation examining w_{sp}, w_{sl}, and the translucency of 3D-printed denture base resins, most materials showed higher w_{sp} values after aging than initially (Gad et al., 2022). Most of the materials furthermore showed higher w_{sl} values in the initial than in the aged group, which may be due to the fact that residual monomers were already dissolved out of the polymer network during the aging process. The emerging voids and the resultant impaired surface properties may explain the increased w_{sp} values after aging. Interestingly, VPR, which initially presented the highest w_{sl}, showed the lowest w_{sl} after aging. While one may thus assume the material to form voids and present a high w_{sp} after aging, VPR was the only material that presented a lower w_{sp} after aging than observed initially, calling for further investigations. In contrast to the expectation that a high *DC* and high mechanical properties would translate into low w_{sp} and w_{sl} values, positive correlations were observed between w_{sp} and *DC*, E_{IT} and *FS, and* w_{sl} and *FS*. This finding underlines the need for a closer examination of the surface properties and the behavior of these materials when in contact with water.

The *DC* of the milled and autopolymerized resins could not be determined. IVO was present in a CAD/CAM blank in the cured state, with no unpolymerized resin available for the requisite initial measurement. For PAL, it was not possible to detect peaks at 1.640 cm^{-1} ((un)polymerized methacrylate C=C stretching mode) and 1.610 cm^{-1} (aromatic C=C stretching mode) to calculate the conversion rate. This limitation requires further research as to why no Raman peaks could be identified between 1200 cm^{-1} – 2000 cm^{-1} for this autopolymerizate, before and after polymerization. The absolute values (74.58–93.00%) observed in this investigation show a very high *DC* of the 3D-printed resins in comparison with previous investigations examining resin composites (Mayinger et al., 2021) and were comparable to those observed for 3D-printed resins for provisional restorations (Mayer et al., 2021). This is a promising finding for this material group, as in theory, a high *DC* should result in a lower solubility of residual monomers and in consequence a higher biocompatibility (Durner et al., 2012; dos Santos et al., 2014), which is especially important with regard to the clinical indication of this material group, where denture bases extensively cover the mucosa and could induce allergic reactions on a big scale. In previous investigations, resins post-cured in a polymerization device using flashes showed a higher conversion rate than those post-cured by the continuous emittance of UV-light (Reymus et al., 2019; Mayinger et al., 2021). The repeated emittance of concentrated flashes possibly results in a higher intensity (Reymus et al., 2019), whereas in the UV lightbox, the objects are exposed to a lower intensity for a longer period of time. In contrast to these investigations (Reymus et al., 2019; Mayinger et al., 2021), this examination observed materials that were post-cured in the UV light box to show the highest degree of conversion regardless of aging. The higher conversion rate following polymerization in the UV box indicates that not only the intensity of the exposure, but also its duration has an influence on the degree of conversion. This is consistent with the finding that the longer the exposure time, the higher the conversion rate (Aati et al., 2022; Kim et al., 2020). As was to be expected, the *DC* showed a positive correlation with the mechanical properties (E_{IT} and *FS)*, which also showed a positive correlation among one another (Aati et al., 2022; Kelch et al., 2022). The fact that three 3D-print resins showed the same *DC* values before and after aging suggests that the light exposure and partly increased temperatures during the aging process have no effect on the conversion rate and that the maximum is already reached after printing and post curing. In contrast to that, VPR showed

higher values after aging, which may either indicate that residual monomers are leached from the material during aging, a finding that is in line with the observe w_{sl} values, or that the material is post-polymerized during the aging process. Since the effects of additional light exposure are highly material-dependent (i. a., on the filler content, the amount of initiators), there is a wide range from no to high impact of additional light exposure on the material's properties (Kelch et al., 2022). As the manufacturers do not provide the exact chemical composition of the examined 3D-printed resins, a comparison of the materials based on their composition was not viable.

The absolute values reported for the E_{IT} are in a similar range as observed previously (2.95–4.09 GPa) (Reymus and Stawarczyk, 2021; Polychronakis et al., 2020). In this investigation, VPR showed the highest E_{IT} values, while FOT and the two control groups showed the lowest values. The E_{IT} values thus agree with previous investigations, where 3D-printed materials showed higher E_{IT} values than a milled control group (Reymus and Stawarczyk, 2021; Polychronakis et al., 2020). The high values observed for VPR and the low values reported for FOT are consistent with the documented conversion rates and the expectation, that a higher *DC* results in a higher stiffness and thus an increased Martens hardness and E_{IT} (Reymus and Stawarczyk, 2020). Only DEN and IVO were susceptible to aging in relation to the reported E_{IT} values and showed higher values when tested initially than after aging, which is in accordance to a previous investigation, where some materials showed lower Martens hardness and E_{IT} values after thermocycling (Hampe et al., 2018). Thermal stresses and water storage may impair the surface quality of resins and result in the absorption of water, as underlined by the increased w_{sp} after aging reported for most materials. This may entail a decrease of the objects' surface properties, such as E_{IT}.

When trying to measure the *ECR* of the two control groups, no chipping occurred, and the Vickers pyramid only left an imprint on the specimens' edge. The low E_{IT} values of these materials, indicating a high elasticity, may, in theory, explain why the material deformed but did not chip. As the control groups did, however, not show significantly lower E_{IT} values than those reported for the 3D-print resins, the resistance to chipping may be tied to another physical property, warranting further research. All 3D-printed materials showed equal properties in regard to chipping. As this property can translate into the ability to withstand crack propagation, an important factor in high load areas of a denture base, the investigated 3D-print materials may be equally suitable to withstand those forces. In comparison with a previous investigation, where PMMA based materials were tested, the 3D-print resins presented lower *ECR* values (Quinn et al., 2014). As the test set-up used for determining *ECR* differs between research groups, i.a. in regard to the employed indenter, future investigations are warranted to compare 3D-print, milled and autopolymerized resins using the same measurement set-up. A variation of the crosshead speed, the applied force, and the distance of the indenter to the edge may result in an expansion of this method that could enable the successful measurement of materials with a similar composition to IVO and PAL. The fact that not all materials could be tested in the present *ECR* set-up, and that this property did not correlate with any of the other investigated parameters, may, however, suggest that the *ECR* measurement is unsuitable for PMMA materials in its current form. Determining the fracture toughness of these materials according to the ISO standard may yield more meaningful results (DIN EN ISO, 20795, 2079). Only one material, FRE, showed lower *ECR* values after aging. This finding agrees with the reported *FS* and a previous investigation, where thermocycling resulted in lower *ECR* values, because hydrolysis and thermal stress led to a degradation of the resin (Zadeh et al., 2021).

All specimens of the IVO groups and a few specimens (4 initial and 5 aged) of the PAL groups did not fracture during the *FS* measurements, as the maximum deflection was reached before breaking. To include PAL and IVO in the statistical analyses, the *FS* values determined at the time when the measurements were stopped were used. This deviation from the ISO norm may indicate this set-up to be unsuitable for resin materials such as IVO or PAL. An alternative to bending tests could be the determination of the tensile strength, which is not limited by the maximum possible deflection due to the geometry of the specimen holder, thus allowing the measurement of highly elastic materials. The initially measured values of all materials reached the minimum values specified in the ISO standards (60 MPa) and may thus be considered as suitable denture base materials (DIN EN ISO, 20795, 2079). In contrast to previous findings where 3D-printed denture base resins showed lower values than CAD/CAM milled and conventional PMMA, this investigation showed the highest *FS* values for FRE and VPR and the lowest for FOT and the two control groups (Perea-Lowery et al., 2021; Prpić et al., 2020). The high values observed for DEN, FRE and VPR in comparison with FOT are mirrored in the reported *DC* and E_{IT} values. The poorer performance of FOT may be linked to an inadequate polymerization, although FRE was successfully polymerized with half the number of flashes, and/or the composition of the resin, as cross-linked polymer chains and inorganic fillers can e.g. result in an increased strength and durability of a material (Alp et al., 2019). The vague composition provided by the manufacturers does, however, not allow a deduction of the observed mechanical properties based on the resins' composition. The low *FS* values reported for PAL and IVO may not be clinically relevant, as the specimens did not break but were deflected. In dependence of the applied force in a clinical situation, the restoration may thus reform to its original state (in the case of an elastic deformation) and still be functional or stay in a deformed state (in the case of a plastic deformation). As seen for w_{sp} and E_{IT}, most materials were impaired by aging and showed higher *FS* values initially than after aging. A water uptake during the aging process can result in plasticization, where water incorporation into the polymer chains leads to an increased movability in the polymer, causing a reduction of the mechanical properties (Aati et al., 2022).

5. Conclusions

The 3D-printed resins showed higher E_{IT} and *FS*, but also higher w_{sp} and w_{sl} values compared to the milled and conventionally manufactured denture base resins. In view of the standards defined by the ISO norm, FOT and FRE represent the 3D-print resin material of choice. As the employed number of thermal cycles only imitates a clinical period of 6 months, the observed findings must be confirmed by long-term in vitro and in vivo investigations. Challenges in the measurement of the *DC*, the *ECR* and the *FS* call for adapted test set-ups. With regard to the promising mechanical properties observed for 3D-printed resins in this investigation, the material and time saving manufacturing by 3D-printing represents a valid addition to the digital fabrication of denture bases.

Within the limitations of this study, the following conclusions can be drawn:

1. The 3D-printed denture base resins showed higher w_{sp} and w_{sl} values than the control groups.
2. Three of the four 3D-printed resins (DEN, FRE and VPR) presented similar or higher E_{IT} and higher *FS* values than those reported for the milled and autopolymerized resins.
3. Within the 3D-printed resins, DEN and VPR showed high *DC*, E_{IT} and *FS*, while FOT showed low w_{sp} values. FOT and FRE were the only 3D-printed materials that met the standards set by the ISO norm.
4. In all materials, the examined parameters were affected by aging. In PAL, aging showed the lowest influence.

CRediT authorship contribution statement

Veronika Greil: Writing – review & editing, Writing – original draft, Visualization, Investigation, Formal analysis, Data curation. **Felicitas Mayinger:** Writing – review & editing, Visualization, Supervision, Methodology. **Marcel Reymus:** Writing – review & editing, Supervision,

Methodology. **Bogna Stawarczyk:** Writing – review & editing, Validation, Supervision, Software, Resources, Project administration, Methodology, Investigation, Formal analysis, Data curation, Conceptualization.

Declaration of competing interest

The authors declare that they have no known competing financial interests or personal relationships that could have appeared to influence the work reported in this paper.

Data availability

Data will be made available on request.

Acknowledgements

The authors thank NextDent, Dreve ProDiMed, DETAX, VOCO, Ivoclar Vivadent and Kulzer for supporting this investigation.

This research did not receive any specific grant from funding agencies in the public, commercial, or not-for-profit sectors.

References

Aati, S., Akram, Z., Shrestha, B., Patel, J., Shih, B., Shearston, K., et al., 2022. Effect of post-curing light exposure time on the physico-mechanical properties and cytotoxicity of 3D-printed denture base material. Dent. Mater. 38, 57–67. https://doi.org/10.1016/j.dental.2021.10.011.

Alharbi, N., Wismeijer, D., Osman, R.B., 2017. Additive manufacturing techniques in prosthodontics: where do we currently stand? A critical review. Int. J. Prosthodont. (IJP) 30, 474–484. https://doi.org/10.11607/ijp.5079.

Alhareb, A.O., Akil, H.M., Ahmad, Z.A., 2017. Impact strength, fracture toughness and hardness improvement of PMMA denture base through addition of nitrile rubber/ceramic fillers. Saudi J.Dent.Res. 8, 26–34. https://doi.org/10.1016/j.sjdr.2016.04.004.

Alp, G., Murat, S., Yilmaz, B., 2019. Comparison of flexural strength of different CAD/CAM PMMA-based polymers. J. Prosthodont. : Off. J.Am. Coll.Prosthodont. 28, e491–e495. https://doi.org/10.1111/jopr.12755.

Bartoloni, J.A., Murchison, D.F., Wofford, D.T., Sarkar, N.K., 2000. Degree of conversion in denture base materials for varied polymerization techniques. J. Oral Rehabil. 27, 488–493. https://doi.org/10.1046/j.1365-2842.2000.00536.x.

Berli, C., Thieringer, F.M., Sharma, N., Müller, J.A., Dedem, P., Fischer, J., et al., 2020. Comparing the mechanical properties of pressed, milled, and 3D-printed resins for occlusal devices. J. Prosthet. Dent 124, 780–786. https://doi.org/10.1016/j.prosdent.2019.10.024.

Bilgin, M.S., Baytaroğlu, E.N., Erdem, A., Dilber, E., 2016. A review of computer-aided design/computer-aided manufacture techniques for removable denture fabrication. Eur. J. Dermatol. 10, 286–291. https://doi.org/10.4103/1305-7456.178304.

Dawood, A., Marti Marti, B., Sauret-Jackson, V., Darwood, A., 2015. 3D printing in dentistry. Br. Dent. J. 219, 521–529. https://doi.org/10.1038/sj.bdj.2015.914.

DIN CEN/TS 843-9:2010-11. Advanced technical ceramics - Mechanical properties of monolithic ceramics at room temperature - Part 9: Method of test for edge-chip resistance.

DIN EN ISO 14577-1: 2015. Metallic materials — Instrumented indentation test for hardness and materials parameters — Part 1: Test method.

DIN EN ISO 20795-1:2013. Dentistry — Base polymers — Part 1: Denture base polymers.

dos Santos, R.L., Sampaio, GA de, Carvalho, FG de, Pithon, M.M., Guênes, G.M., Alves, P. M., 2014. Influence of degree of conversion on the biocompatibility of different composites in vivo. J. Adhesive Dent. 16, 15–20. https://doi.org/10.3290/j.jad.a29704.

Durner, J., Obermaier, J., Draenert, M., Ilie, N., 2012. Correlation of the degree of conversion with the amount of elutable substances in nano-hybrid dental composites. Dent. Mater. 28, 1146–1153. https://doi.org/10.1016/j.dental.2012.08.006.

Gad, M.M., Alshehri, S.Z., Alhamid, S.A., Albarrak, A., Khan, S.Q., Alshahrani, F.A., et al., 2022. Water sorption, solubility, and translucency of 3D-printed denture base resins. Dent. J. 10 https://doi.org/10.3390/dj10030042.

Gale, M., Darvell, B., 1999. Thermal cycling procedures for laboratory testing of dental restorations. J. Dent. 27, 89–99. https://doi.org/10.1016/s0300-5712(98)00037-2.

Hada, T., Kanazawa, M., Iwaki, M., Katheng, A., Minakuchi, S., 2021. Comparison of mechanical properties of PMMA disks for digitally designed dentures. Polymers 13, 1745. https://doi.org/10.3390/polym13111745.

Hampe, R., Lümkemann, N., Sener, B., Stawarczyk, B., 2018. The effect of artificial aging on Martens hardness and indentation modulus of different dental CAD/CAM restorative materials. J. Mech. Behav. Biomed. Mater. 86, 191–198. https://doi.org/10.1016/j.jmbbm.2018.06.028.

Kelch, M., Stawarczyk, B., Mayinger, F., 2022. Chemical and mechanical properties of dual-polymerizing core build-up materials. Clin. Oral Invest. https://doi.org/10.1007/s00784-022-04455-4.

Kessler, A., Hickel, R., Reymus, M., 2020. 3D printing in dentistry-state of the art. Operat. Dent. 45, 30–40. https://doi.org/10.2341/18-229-L.

Kim, D., Shim, J.-S., Lee, D., Shin, S.-H., Nam, N.-E., Park, K.-H., et al., 2020. Effects of post-curing time on the mechanical and color properties of three-dimensional printed crown and bridge materials. Polymers 12. https://doi.org/10.3390/polym12112762.

Kraemer Fernandez, P., Unkovskiy, A., Benkendorff, V., Klink, A., Spintzyk, S., 2020. Surface characteristics of milled and 3D printed denture base materials following polishing and coating: an in-vitro study. Materials 13. https://doi.org/10.3390/ma13153305.

Li, P., Krämer-Fernandez, P., Klink, A., Xu, Y., Spintzyk, S., 2021. Repairability of a 3D printed denture base polymer: effects of surface treatment and artificial aging on the shear bond strength. J. Mech. Behav. Biomed. Mater. 114, 104227 https://doi.org/10.1016/j.jmbbm.2020.104227.

Mayer, J., Reymus, M., Wiedenmann, F., Edelhoff, D., Hickel, R., Stawarczyk, B., 2021. Temporary 3D printed fixed dental prosthesis materials: impact of post printing cleaning methods on degree of conversion as well as surface and mechanical properties. Int. J. Prosthodont. (IJP) 34, 784–795. https://doi.org/10.11607/ijp.7048.

Mayinger, F., Reymus, M., Liebermann, A., Richter, M., Kubryk, P., Großekappenberg, H., et al., 2021. Impact of polymerization and storage on the degree of conversion and mechanical properties of veneering resin composites. Dent. Mater. J. 40, 487–497. https://doi.org/10.4012/dmj.2019-394.

Oliveira Limírio, JPJ de, Gomes, JMdL., Alves Rezende, M.C.R., Lemos, C.A.A., Del Rosa, C.D.R.D., Pellizzer, E.P., 2021. Mechanical properties of polymethyl methacrylate as a denture base: conventional versus CAD-CAM resin - a systematic review and meta-analysis of in vitro studies. J. Prosthet. Dent. https://doi.org/10.1016/j.prosdent.2021.03.018.

Perea-Lowery, L., Gibreel, M., Vallittu, P.K., Lassila, L.V., 2021. 3D-Printed vs. Heat-polymerizing and autopolymerizing denture base acrylic resins. Materials 14. https://doi.org/10.3390/ma14195781.

Polychronakis, N., Dimitriadi, M., Ioannidis, A., Papadopoulos, T., 2020. The effect of different cooling procedures on mechanical properties of denture base materials measured by instrumented indentation testing. J. Prosthodont. Restor. 64, 326–331. https://doi.org/10.1016/j.jpor.2019.09.005.

Prpić, V., Schauperl, Z., Ćatić, A., Dulčić, N., Čimić, S., 2020. Comparison of mechanical properties of 3D-printed, CAD/CAM, and conventional denture base materials. J. Prosthodont. : Off. J.Am. Coll.Prosthodont. 29, 524–528. https://doi.org/10.1111/jopr.13175.

Quinn, G.D., Giuseppetti, A.A., Hoffman, K.H., 2014. Chipping fracture resistance of denture tooth materials. Dent. Mater. 30, 545–553. https://doi.org/10.1016/j.dental.2014.02.011.

Reymus, M., Stawarczyk, B., 2020. Influence of different postpolymerization strategies and artificial aging on hardness of 3D-printed resin materials: an in vitro study. Int. J. Prosthodont. (IJP) 33, 634–640. https://doi.org/10.11607/ijp.6634.

Reymus, M., Stawarczyk, B., 2021. In vitro study on the influence of postpolymerization and aging on the Martens parameters of 3D-printed occlusal devices. J. Prosthet. Dent 125, 817–823. https://doi.org/10.1016/j.prosdent.2019.12.026.

Reymus, M., Lümkemann, N., Stawarczyk, B., 2019. 3D-printed material for temporary restorations: impact of print layer thickness and post-curing method on degree of conversion. Int. J. Comput. Dent. 22, 231–237.

Strub, J.R., Rekow, E.D., Witkowski, S., 2006. Computer-aided design and fabrication of dental restorations: current systems and future possibilities. J. Am. Dent. Assoc. 137, 1289–1296. https://doi.org/10.14219/jada.archive.2006.0389.

Tian, Y., Chen, C., Xu, X., Wang, J., Hou, X., Li, K., et al., 2021. A review of 3D printing in dentistry: technologies, affecting factors, and applications. Scanning 2021, 9950131. https://doi.org/10.1155/2021/9950131.

Whitley, D., Eidson, R.S., Rudek, I., Bencharit, S., 2017. In-office fabrication of dental implant surgical guides using desktop stereolithographic printing and implant treatment planning software: a clinical report. J. Prosthet. Dent 118, 256–263. https://doi.org/10.1016/j.prosdent.2016.10.017.

Zadeh, P.N., Stawarczyk, B., Hampe, R., Liebermann, A., Mayinger, F., 2021. Edge chipping resistance of veneering composite resins. J. Mech. Behav. Biomed. Mater. 116, 104349 https://doi.org/10.1016/j.jmbbm.2021.104349.

Zafar, M.S., 2020. Prosthodontic applications of polymethyl methacrylate (PMMA): an update. Polymers 12. https://doi.org/10.3390/polym12102299.

Veröffentlichung II

journal of the mechanical behavior of biomedical materials 150 (2024) 106234

Contents lists available at ScienceDirect

Journal of the Mechanical Behavior of Biomedical Materials

journal homepage: www.elsevier.com/locate/jmbbm

Fracture toughness, work of fracture, flexural strength and elastic modulus of 3D-printed denture base resins in two measurement environments after artificial aging

Veronika Geiger [a,*,1], Felicitas Mayinger [a,1], Moritz Hoffmann [a], Marcel Reymus [b], Bogna Stawarczyk [a]

[a] Department of Prosthetic Dentistry, Dental School, LMU Munich, Goethestraße 70, 80336, Munich, Germany
[b] Department of Conservative Dentistry and Periodontology, Dental School, LMU Munich, Goethestraße 70, 80336, Munich, Germany

ARTICLE INFO

Keywords:
Denture base resin
Fracture toughness
Flexural strength
Additive technology
3D-printing

ABSTRACT

Objectives: To investigate the fracture toughness (K_{IC}), work of fracture (WOF), flexural strength (FS) and elastic modulus (E) of four additively manufactured denture base resins in two different measurement environments after artificial aging.

Methods: Rectangular specimens in two different dimensions (n = 480) were 3D-printed with four denture base resins: Denture 3D+ (DEN; NextDent), Fotodent Denture (FOT; Dreve ProDiMed), Freeprint Denture (FRE; Detax), V-Print dentbase (VPR; VOCO)). K_{IC}, WOF, FS and E were measured after (1) water-storage (37 °C; K_{IC} = 7 d; FS = 50 h); (2) water-storage + hydrothermal-aging (20 min, 0.2 MPa, 134 °C); (3) water storage + thermocycling (10,000 cycles, 5/55 °C) in two measurement environments (i) air-23 °C and (ii) water-37 °C. For FS, fracture types were classified, and relative frequencies determined. Univariate ANOVA, Kruskal–Wallis, Mann–Whitney U, and Spearman's correlation were calculated ($p < 0.05$, SPSS V.27.0). Weibull modulus (*m*) was calculated using the maximum likelihood estimation method.

Results: DEN showed the highest K_{IC} (5/6 groups), WOF and highest corresponding *m* (1/6 groups), while FRE presented the highest FS (2/6 groups) and E values. Hydrothermal-aging and thermocycling reduced K_{IC} and WOF, FS and E, and the number of FS fracture pieces. For 6/8 groups, hydrothermal aging resulted in lower FS than thermocycling. Measurement in air-23 °C led to higher FS for 7/12 groups and a more brittle fracture behavior. A positive correlation between K_{IC} and FS was observed.

Significance: With measurements in air-23 °C resulting in higher FS than reported in water-37 °C, the measurement environment should be adapted to the clinical situation to allow valid predictions on the mechanical behavior of denture base resins when in situ.

1. Introduction

Computer-aided design/computer-aided manufacturing (CAD/CAM) technology has been used since the 1980s and improved the versatility, accuracy and cost effectiveness of dental devices (Duret and Preston, 1991). All three elements of the CAD/CAM technology, namely data acquisition, data processing and manufacturing, improved by the increase of computing power, making CAD/CAM a vital part in modern laboratories and clinical dentistry today (van Noort, 2012). This technology often refers to subtractive manufacturing methods, for which the objects are milled out of a solid block until achieving the deigned shape by using multi-axial machines to remove the excess parts. However, some complex geometries cannot be fully reproduced, the material loss is up to 90% and a high wear of the milling burs is observed that demands a renewal of these tools after a short time (Reymus et al., 2020).

In contrast, with additive manufacturing, also known as 3D-printing, the objects are built up layer-by-layer, allowing high precision, realization of complex dimensions, e.g., the incorporation of internal hollows, and a reduction of material waste (Aati et al., 2022; Bilgin et al., 2016; Alharbi et al., 2017). 3D-printing can be easily integrated into the

* Corresponding author. Department of Prosthetic Dentistry Dental school, LMU Munich Goethestrasse 70, 80336, Munich, Germany.
E-mail address: veronika.greil@med.uni-muenchen.de (V. Geiger).
[1] Veronika Geiger and Felicitas Mayinger contributed equally to this work.

https://doi.org/10.1016/j.jmbbm.2023.106234
Received 28 September 2023; Received in revised form 5 November 2023; Accepted 7 November 2023
Available online 10 November 2023
1751-6161/

digital workflow, which results in time savings in the manufacturing process and patient treatment compared to conventional manufacturing methods. Common additive manufacturing methods include fused deposition modelling (FDM), selective laser sintering (SLS), polyjet printing, bioprinting and the most used technique in dentistry as of today, VAT-polymerization, including stereolithography (SLA) and digital light processing (DLP) (Oberoi et al., 2018). In VAT-polymerization, liquid resins are cured by a laser (SLA) or light from a projector (DLP).

While the additive manufacturing of temporary and definitive fixed dental prostheses (FDPs) such as inlays, onlays and crowns has been investigated for several years, the additive fabrication of removable dental protheses (RDPs) has recently moved into the focus of in-vitro and clinical investigations (Miyazaki et al., 2009; Webb, 2000; Sun and Zhang, 2012). Additively manufactured denture bases must show adequate mechanical properties to withstand forces occurring during function, a high biocompatibility as they are in direct extensive contact with the mucosa, and color- and dimensional stability over time. Fracture toughness (K_{IC})/work of fracture (WOF) and flexural strength (FS)/elastic modulus (E) are critical properties specified in the ISO (International Organization for Standardization) standard for polymer-based materials (ISO, 20795–1:2013) (ISO, 20795–1, 2013), that can be used to predict the clinical performance of the examined materials (Oliveira Limírio JPJ de et al., 2021). While K_{IC} can quantify a material's resistance against the propagation of pre-existing cracks, e.g., running along the middle of the prosthesis where peak forces in the posterior regions result in the formation of tensile stresses, FS may yield information about a denture's resistance against plastic deformation and fracture during loading and thus aid in the determination of the long-term integrity of RDPs. For reproducing the intraoral environment under standardized laboratory conditions, 10,000 thermal cycles between 5 °C and 55 °C and hydrothermal aging at 134 °C, 0.2 MPa and 20 min were employed to simulate a clinical condition after one year in vivo (Gale and Darvell, 1999; Li et al., 2021a; Chevalier, 2006). While the ISO norm (ISO, 20795–1, 2013) specifies FS to be measured in conditions that imitate the oral environment (37 ± 1 °C and in water), K_{IC} is measured at room temperature (23 ± 1 °C) and at air. To the authors' best knowledge, the impact of the measurement environment on the examined properties has not yet been investigated.

Consequently, the aim of this investigation was to examine the influence of artificial aging and the measurement environment on the mechanical properties of four 3D-printed denture base resin materials. The tested null hypotheses stated that neither the choice of material, artificial aging nor the measurement environment showed an impact on K_{IC} and WOF (including the Weibull modulus *m*) or FS and E (including *m*). Furthermore, it was assumed that the mechanical properties would correlate with each other.

2. Materials and methods

The fracture toughness, work of fracture, flexural strength and elastic modulus of four 3D-printed denture base resin were examined (Fig. 1).

Specimens were designed as rectangular blocks and additively manufactured subsequently (N = 480; n = 120) from different denture base resins (Denture 3D+, abbreviation: DEN, LotNo: WY062N04, NextDent, Soesterberg, Netherlands; Fotodent Denture, FOT, LotNo: 010086X1, Dreve ProDiMed, Unna, Germany; Freeprint Denture, FRE, LotNo: 231007, DETAX, Ettlingen, Germany; V-Print dentbase, VPR, LotNo: 2113368, VOCO, Cuxhaven, Germany) using a DLP 3D-printer (Rapidshape D20 II, Rapid Shape, Heimsheim, Germany). Post-processing was performed according to each manufacturer's instruction (Table 1).

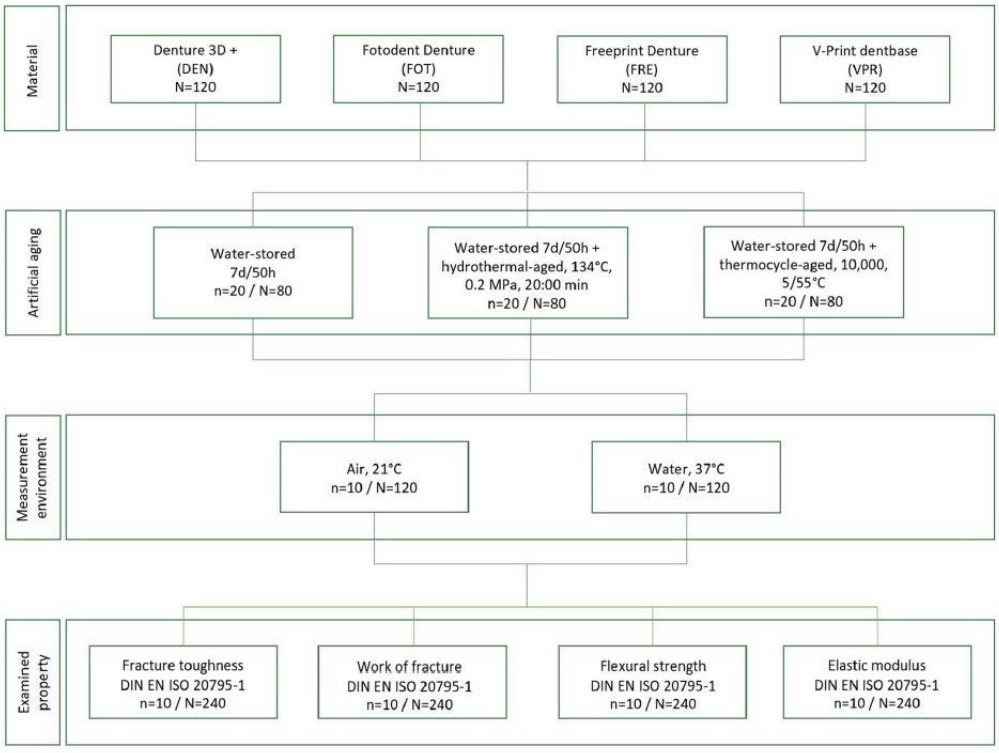

Fig. 1. Study design.

Table 1
Printing, post-processing and post-curing parameters and composition of the different denture base resins.

	Printing parameters	Post-processing	Post-curing	Composition
DEN	50 μ m layer thickness 90° tilted orientation	Ethanol + ultrasonic bath Pre-cleaning: 3 min Final Cleaning: 2 min ethanol	LC-3DPrint Box (NextDent): six 1.7 W UV- and six 2.3 W UV-lamps 315–550 nm Peaks at 360 + 435 nm 30 min	- Ethoxylated bisphenol A dimethacrylate (>75%) - 7,7,9(7,9,9)- trimethyl-4,13-dioxo-3,14-dioxa-5,12-diazahexadecane-1,16-diyl bismethacrylate (10–20%) - 2-hydroxyethyl methacrylate (5–10%) - Silicon dioxide (1–5%) - Diphenyl (2,4,6-trimethylbenzoyl) phosphine Oxide (1–5%) - Titanium dioxide (<0,1%)
FOT		Isopropanol + ultrasonic bath Pre-cleaning: 2 min Final cleaning: 2 min	Otoflash G171 (NK-Optics): 1.4W/cm^2 per flash 280–580 nm Peaks at 480 + 530 nm 2x4000 flashes under nitrogen atmosphere 10 min in an oven (BE500, Memmert, Schwabach, Germany) at 90 °C	- Neopentyl glycol(PO)2 diacrylate (25–50%) - Aliphatic urethane dimethacrylate (25–50%) - Aliphatic urethane trimethacrylate (10–25%) - Diphenyl (2,4,6-trimethylbenzoyl) phosphine Oxide (<2,5%) - Color pigment concentrate (<2,5%)
FRE		Isopropanol + ultrasonic bath Pre-cleaning: 3 min Final cleaning: 3 min	Otoflash G171 (NK-Optics): 1.4W/cm^2 per flash 280–580 nm Peaks at 480 + 530 nm 2x2000 flashes under nitrogen atmosphere	- Isopropylidenediphenol Peg-2 dimethacrylate (35–60%) - 7,7,9(7,9,9)- trimethyl-4,13-dioxo-3,14-dioxa-5,12-diazahexadecane-1,16-diyl bismethacrylate (30–35%) - 2-hydroxyethyl methacrylate (1–5%) - Diphenyl (2,4,6-trimethylbenzoyl) phosphine Oxide (1–5%) - Hydroxypropyl methacrylate (1–5%) - 1,6-hexandiol dimethacrylate (1–5%) - Phenylbis (2,4,6-trimethylbenzoyl) phosphine oxide (<1%)
VPR		Isopropanol + ultrasonic bath Pre-cleaning: 3 min Final Cleaning 2 min	LC-3DPrint Box (NextDent): six 1.7 W UV- and six 2.3 W UV-lamps 315–550 nm Peaks at 360 + 435 nm 30 min	- Aliphatic urethane dimethacrylate (50–100%) - Ethoxylated bisphenol A dimethacrylate (25–50%) - Triethylene glycol dimethacrylate (5–10%) - Diphenyl (2,4,6-trimethylbenzoyl) phosphine Oxide (<2,5%)

Specimens were polished to their final dimensions (Abramin, Struers, Ballerup, Denmark) with a series of silicon carbide papers from P500 up to P1200 under water-cooling and cleaned in an ultrasonic bath (L&R Transistor/Ultrasonic T-14, L&R Ultrasonics, New Jersey, USA) with distilled water. The final dimensions of each specimen (for K_{IC}: 4.0 ± 0.2 mm × 8.0 ± 0.2 mm × 39.0 mm; for FS: 3.3 ± 0.2 mm × 10.0 ± 0.2 mm × 64.0 mm) were verified with a digital micrometer screw with an accuracy of ±4 μm (IP65, Mitutoyo, Kawasaki, Japan). The specimens of each material were divided into three different aging subgroups:

1) Water-stored: storage in 37 °C tempered water (HERAcell 150, Thermo Fisher Scientific, Waltham, USA) for 50 h (FS specimens) or 7 d (K_{IC} specimens)
2) Hydrothermal-aged: storage in 37 °C tempered water for 50 h/7 d and hydrothermal aging for 20 min (0.2 MPa, 134 °C; Euroklav 29-S, MELAG Medizintechnik, Berlin, Germany)
3) Thermocycle-aged: storage in 37 °C tempered water for 50 h/7 d and 10,000x thermal cycles (5/55 °C with a dwell time of 30 s; Thermocycler THE-1100, SD Mechatronik, Feldkirchen-Westerham, Germany)

Each subgroup was tested in two measurement environments, namely:

a) air at 23 °C (specimens were conditioned in 23 °C tempered water for 60 min prior to measurement) or
b) water at 37 °C (after a temperature equilibrium was reached).

K_{IC} and FS were measured in an universal testing machine (1445 Zwick/Roell, Ulm, Germany). WOF and E were calculated from the load-deflection curves.

2.1. Fracture toughness and work of fracture measurement

For K_{IC} measurements, the notch was prepared according to the specifications stated in DIN EN ISO 20795–1:2013. Specimens were placed and fixed in an adjusted specimen holder for an universal cutting machine (Secotom-50, Struers) and the cut was inserted using a diamond cut-off wheel (150 μm, M0D08, Struers) at a displacement speed of 0.05 mm/min and a speed rotation of 5000 rpm. A notch was inserted with a custom-made notch machine on the bottom of the cut using a sharp razor blade (LUTZ, Solingen, Germany). The dimensions of the cut (3.0 ± 0.2 mm) and notch (0.1–0.4 mm) were verified microscopically (Fig. 2, Keyence VHX-970F, Keyence, Osaka, Japan). Each specimen was centrally placed in a specimen holder for 3-point FS measurements with the notch pointing downwards, and K_{IC} was measured at a crosshead speed of 1 mm/min in a displacement-controlled mode until fracture occurred. To determine the exact depth of each notch, the fracture surface was measured post testing using a digital light microscope (Keyence VHX-970F). For each specimen, K_{IC} was calculated using the following equation:

$$K_{IC} = \frac{f P_{max} l_t}{\left(b_t h_t^{3/2}\right)} \bullet \sqrt{10^{-3}}$$

with K_{IC}: fracture toughness ($MPa \bullet m^{1/2}$); P_{max}: fracture load (N); l_t: span (mm); b_t: specimen width (mm); h_t: specimen height (mm); f: a geometric function of x.

$$f(x) = 3x^{1/2}\frac{[1.99 - x(1-x)(2.15 - 3.93x + 2.7x^2)]}{\left[2(1+2x)(1-x)^{3/2}\right]}$$

and

$$x = \frac{a}{h_t}$$

with a: sum of cut depth a' (mm) and notch depth (mm).

The WOF was calculated from the integral area of the load-deflection curve:

$$W_f = \frac{U}{[2b_t(h_t - a)]} \times 1000$$

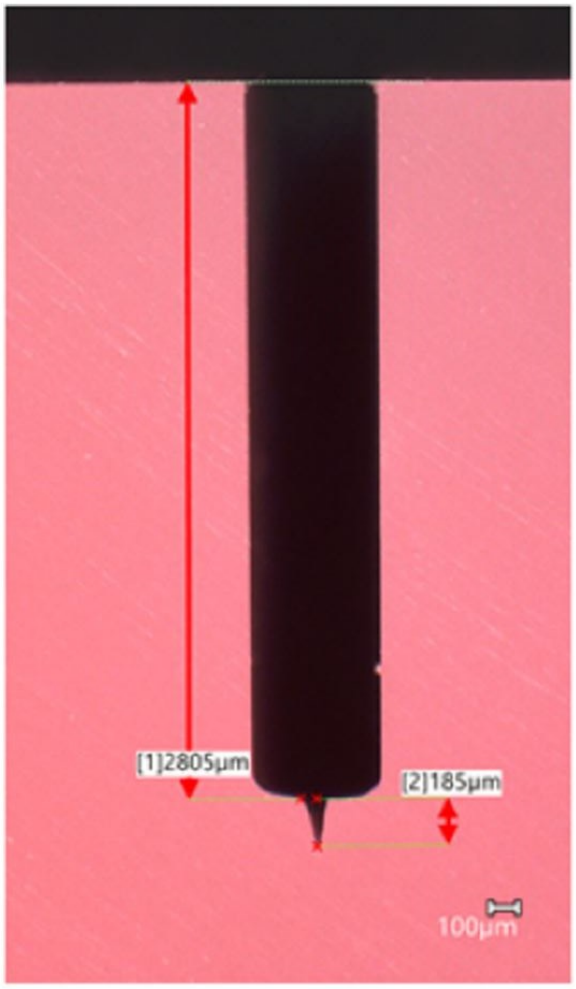

Fig. 2. A specimen prepared for fracture toughness measurement.

and

$$U = \int P d\Delta$$

With W: work of fracture (J/m^2); U: plotted area under the load-deflection curve (Nmm); h_t: specimen height (mm); a: sum of cut depth a' (mm) and notch depth (mm).

2.2. Flexural strength and elastic modulus measurement and fractographic analysis

For 3-point FS measurement, the specimens were centrally placed in the specimen holder for 3-point flexural strength measurements and the FS was measured at a crosshead speed of 5 mm/min in a displacement-controlled mode until fracture or maximum displacement of 10 mm occurred (Fig. 3). The 3-point FS was calculated:

$$\sigma = \frac{3Fl}{2bh^2}$$

with F: fracture load (N); l: span (mm); b_t: specimen width (mm); h_t: specimen height (mm).

E was calculated:

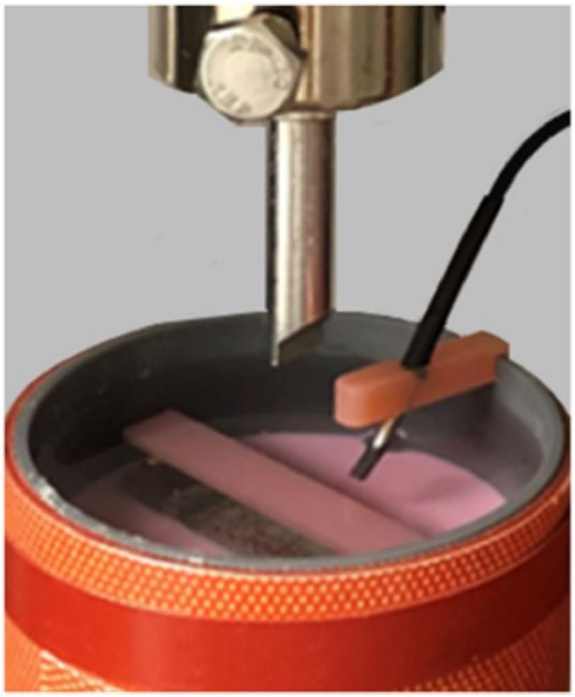

Fig. 3. Set-up for measuring at 37 °C under water.

$$E = \frac{F_1 l^3}{4bh^3 d} \div 1000$$

With E: elastic modulus (GPa); F_1: load (N) at point in the straight portion (at maximum slope) of the load-deflection curve; d: deflection at F_1 (mm); l: span (mm); b: specimen width (mm); h: specimen height (mm). Fig. 4 shows a typical load-deflection curve for a DEN specimen after water-storage tested in air 23 °C.

Fractographic analyses were performed at a 20 × – 1000× magnification using a digital light microscope (Keyence VHX-970F, Keyence, Osaka, Japan). Fracture types were classified as *(1) a* deformation of the specimen (Fig. 5a), *(2) a* fracture between the printing layers resulting

Fig. 4. Load-deflection curve of a water-stored DEN specimen tested in air 23 °C.

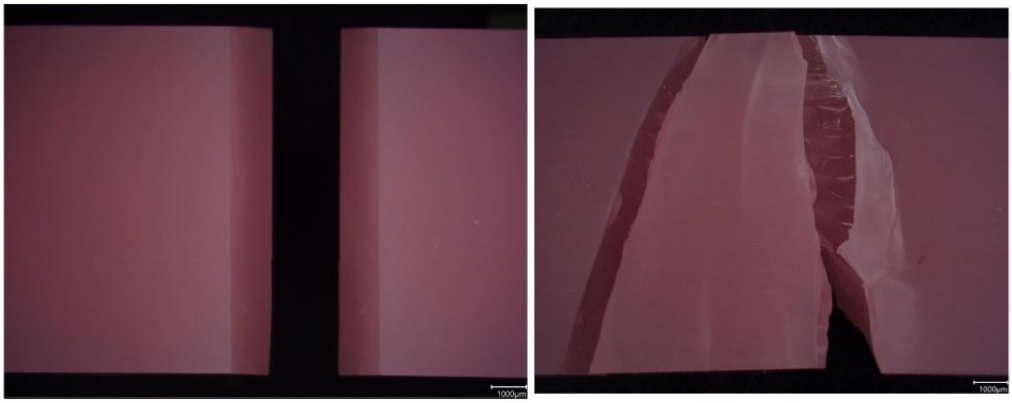

Fig. 5. Fracture types a. deformation of the specimen, b. 90° fracture between the printing layers resulting in two fracture pieces, c. complex fracture into ≥3 parts.

in two fracture pieces (Fig. 5b) and *(3)* a complex fracture into ≥3 parts (Fig. 5c).

2.3. Statistical analyses

Statistical analyses were computed with the SPSS statistics program (V.27.0, IBM, Armonk, USA). The deviation from the normal distribution of the data was verified using the Kolmogorov–Smirnov test. For global analyses, univariate ANOVA with partial eta squared (η_p^2) was used. Kruskal–Wallis and Mann–Whitney *U* test were computed to determine significant differences between the different material, artificial aging, and measurement environment groups. Spearman's correlation was calculated to examine the association between K_{IC}, WOF, FS and E. Two-parameter Weibull analysis using the maximum likelihood estimation method at a 95% confidence level was used to estimate the reliability of the observed K_{IC} and FS values (Roos and Stawarczyk, 2012). Fracture types were classified, and relative frequencies were computed using a Ciba-Geigy table. All p-values ≤0.05 were considered as significant.

3. Results

A deviation from the normal distribution for 12.5% (3/24) of the K_{IC}, 25% (6/24) of the WOF, 37.5% (9/24) of FS and 16.7% (4/24) of the E groups was observed. Therefore, all data were analyzed non-parametrically.

Table 2
Descriptive statistics for K_{IC} ($MPa^a m^{1/2}$) and WOF (J/m^2) with mean, standard deviation (SD) and 95% confidence interval (CI)) and Weibull modulus *m* with 95% CI.

		DEN		FOT		FRE		VPR	
		Mean ± SD	95% CI	Mean ± SD	95% CI	Mean ± SD	95% CI	Mean ± SD	95% CI
water-stored									
Air, 23 °C	K_{IC}	$0.98 \pm 0.03^{c,B,\beta}$	(0.95; 1.00)	$0.71 \pm 0.04^{a,B,\alpha}$	(0.66; 0.75)	$0.71 \pm 0.09^{aa,B,\alpha}$	(0.63; 0.78)	$0.91 \pm 0.06^{b,B,\beta}$	(0.86; 0.96)
	WOF	$95.4 \pm 5.7^{d,A,\alpha}$	(91.1; 99.5)	$65.9 \pm 4.4^{ab,B,\alpha}$	(61.7; 70.1)	$49,6 \pm 13.3^{a,B,\alpha}$	(40.0; 59.2)	$76.8 \pm 8.7^{c,B,\alpha}$	(70.4; 83.1)
	m	$44.8^{b,B,\alpha}$	(23.2; 85.9)	$18.7^{a,B,\alpha}$	(9.6; 35.8)	$12.0^{a,A,\alpha}$	(6.1; 22.7)	$20.4^{a,B,\alpha}$	(10.5; 39.1)
Water, 37 °C	K_{IC}	$0.92 \pm 0.04^{c,B,\alpha}$	(0.87; 0.95)	$0.81 \pm 0.05^{a,B,\beta}$	(0.74; 0.88)	$0.82 \pm 0.11^{abc,B,\beta}$	(0.73; 0.90)	$0.83 \pm 0.04^{b,B,\alpha}$	(0.79; 0.87)
	WOF	$130.6 \pm 9.3^{c,B,\beta}$	(124.0; 137.3)	$89.1 \pm 10.3^{b,B,\beta}$	(76.2; 101.9)	$81.8 \pm 29.9^{ab,B,\beta}$	(60.3; 103.3)	$74.0 \pm 6.6^{a,A,\alpha}$	(69.2; 78.8)
	m	$25.3^{b,A,\alpha}$	(13.1; 48.5)	$15.3^{ab,B,\alpha}$	(7.8; 29.4)	$9.8^{a,A,\alpha}$	(5.0; 18.9)	$22.6^{b,B,\alpha}$	(11.6; 43.3)
hydrothermal-aged									
Air, 23 °C	K_{IC}	$0.94 \pm 0.03^{d,A,\beta}$	(0.91; 0.96)	$0.70 \pm 0.04^{b,B,\alpha}$	(0.66; 0.74)	$0.53 \pm 0.02^{a,A,\alpha}$	(0.50; 0.55)	$0.75 \pm 0.04^{c,A,\alpha}$	(0.71; 0.79)
	WOF	$105.6 \pm 10.3^{d,B,\alpha}$	(98.1; 113.0)	$74.8 \pm 11.0^{ac,B,\alpha}$	(66.2; 83.3)	$31.2 \pm 2.9^{a,A,\alpha}$	(29.0; 33.4)	$60.6 \pm 7.0^{b,A,\alpha}$	(55.5; 65.6)
	m	$45.1^{b,B,\beta}$	(23.4; 86.4)	$20.3^{a,B,\alpha}$	(10.4; 38.9)	$25.6^{a,B,\beta}$	(13.2; 49.2)	$21.6^{a,B,\alpha}$	(11.1; 41.5)
Water, 37 °C	K_{IC}	$0.84 \pm 0.05^{c,A,\alpha}$	(0.79; 0.89)	$0.75 \pm 0.07^{ab,B,\alpha}$	(0.66; 0.83)	$0.69 \pm 0.08^{a,A,\beta}$	(0.61; 0.76)	$0.79 \pm 0.03^{ab,A,\beta}$	(0.76; 0.82)
	WOF	$122.5 \pm 9.5^{c,AB,\beta}$	(115.6; 129.4)	$81.1 \pm 16.4^{b,B,\alpha}$	(63.7; 98.4)	$53.3 \pm 11.9^{a,A,\beta}$	(44.7; 61.9)	$81.6 \pm 7.6^{b,B,\beta}$	(76.1; 87.1)
	m	$18.8^{b,A,\alpha}$	(9.7; 36.0)	$12.8^{ab,AB,\alpha}$	(6.5; 24.5)	$9.0^{a,A,\alpha}$	(4.5; 17.3)	$31.9^{b,B,\alpha}$	(16.5; 61.1)
thermocycle-aged									
Air, 23 °C	K_{IC}	$0.98 \pm 0.08^{b,AB,\beta}$	(0.91; 1.04)	$0.65 \pm 0.09^{a,A,\alpha}$	(0.56; 0.72)	$0.66 \pm 0.14^{a,B,\alpha}$	(0.55; 0.76)	$0.74 \pm 0.15^{a,A,\alpha}$	(0.62; 0.85)
	WOF	$113.1 \pm 26.3^{ac,B,\alpha}$	(94.1; 132.0)	$55.3 \pm 16.8^{ab,A,\alpha}$	(42.2; 68.2)	$46.1 \pm 20.9^{aab,B,\alpha}$	(31.0; 61.1)	$62.2 \pm 22.6^{b,AB,\alpha}$	(45.9; 78.4)
	m	$16.5^{b,A,\alpha}$	(8.5; 31.7)	$8.5^{ab,A,\alpha}$	(4.3; 16.4)	$7.5^{a,A,\alpha}$	(3.8; 14.4)	$6.3^{a,A,\alpha}$	(3.1; 12.0)
Water, 37 °C	K_{IC}	$0.84 \pm 0.04^{c,A,\alpha}$	(0.80; 0.87)	$0.57 \pm 0.06^{a,A,\alpha}$	(0.51; 0.63)	$0.68 \pm 0.06^{b,A,\alpha}$	(0.62; 0.73)	$0.74 \pm 0.09^{ab,A,\alpha}$	(0.66; 0.81)
	WOF	$115.5 \pm 9.6^{c,A,\alpha}$	(108.5; 122.4)	$51.0 \pm 7.4^{a,A,\alpha}$	(44.0; 57.9)	$48.9 \pm 9.0^{a,A,\alpha}$	(42.3; 55.3)	$69.7 \pm 17.5^{ab,AB,\alpha}$	(57.0; 82.2)
	m	$26.4^{b,A,\alpha}$	(13.6; 50.5)	$7.7^{a,A,\alpha}$	(3.8; 14.7)	$14.5^{a,A,\alpha}$	(7.4; 27.8)	$10.9^{a,A,\alpha}$	(5.6; 21.0)

^{a,b,c,d} indicate significant differences between materials within one aging level and one measurement environment.
^{A,B,C} indicate significant differences between aging levels within one material and one measurement environment.
$^{\alpha,\beta}$ indicate significant differences between measurement environments within one aging level and one material.
CI=Confidence Interval.
SD= Standard Deviation.
[a] Deviation from the normal distribution.

3.1. Fracture toughness and work of fracture

Due to the interactions between the variables (partial eta-squared (η_p^2) = 0.067–0.205, p < 0.001), the results were split and analyzed separately.

3.1.1. Impact of the material on fracture toughness and work of fracture

Within the water-stored group tested in air-23 °C, DEN showed the highest K_{IC}, followed by VPR, while FOT and FRE showed the lowest values (p < 0.001–0.119) (Table 2, Fig. 6). DEN showed higher *m* values than the other materials. When tested in water-37 °C, DEN showed the highest K_{IC}, followed by VPR, with FOT showing lower values (p < 0.001–0.545). DEN and VPR presented the highest *m* and FRE the lowest.

After hydrothermal-aging and testing in air-23 °C, DEN showed the highest K_{IC} values, followed by VPR, FOT and FRE (p < 0.001–0.023). DEN showed higher *m* than FOT and VPR. When tested in water-37 °C, DEN had the highest K_{IC} values, followed by VPR and FOT (p = 0.001–0.257). DEN and VPR showed higher *m* than FRE.

Within the thermocycle-aged group tested in air-23 °C, DEN showed higher K_{IC} values than FOT, FRE and VPR (p < 0.001–0.999). DEN showed higher *m* than VPR and FRE. When tested in water-37 °C, DEN had the highest K_{IC}, followed by FRE and VPR, while FOT showed the lowest values (p < 0.001–0.199). DEN showed higher *m* than FOT and VPR.

In all tested groups, DEN showed the highest and FRE the lowest WOF values (p < 0.001–0.821)

3.1.2. Impact of artificial aging on fracture toughness and work of fracture

For groups tested in air-23 °C, DEN and FRE showed higher K_{IC} and FRE also higher WOF values after water storage and thermocycling than after hydrothermal aging. DEN, on the other hand, showed higher WOF values after hydrothermal aging and thermocycling (p = 0.007–0.821). For FOT, water storage and hydrothermal aging led to higher K_{IC} and WOF values than observed after thermocycling (p < 0.001–0.940). VPR showed the highest values after water-storage (p < 0.001–0.496). For DEN, FOT and VPR, water storage and hydrothermal aging resulted in higher *m* than observed after thermocycling. FRE showed the highest *m* after hydrothermal aging.

For groups tested in water-37 °C, DEN, FRE and VPR showed the highest K_{IC} and DEN and FRE also the highest WOF values after water storage (p < 0.001–0.999). FOT showed the highest values after water-storage and hydrothermal-aging (p < 0.001–0.545). VPR showed the highest WOF values after hydrothermal aging and thermocycling (p < 0.001–0.545). For FOT, water-storage led to higher *m* than thermocycling. For VPR, the water-stored and hydrothermal-aged groups showed higher *m* than the thermocycle-aged group.

3.1.3. Impact of the measurement environment on fracture toughness and work of fracture

Water-stored DEN and VPR showed higher K_{IC} when examined in air-23 °C than in water-37 °C (p = 0.001–0.002). Within FOT and FRE, groups examined in water-37 °C showed higher K_{IC} than those tested in air-23 °C(p = 0.005–0.023).

After hydrothermal aging, FRE and VPR showed higher K_{IC} when tested in water-37 °C than in air-23 °C (p < 0.001–0.016). For DEN and FRE, measurement in air-23 °C led to higher *m* than measurements in water-37 °C.

Both after hydrothermal aging and thermocycling, DEN showed higher K_{IC} when examined in air-23 °C than in water-37°(p < 0.001).

Water stored and hydrothermal aged groups showed higher WOF values when tested in water (p < 0.001–0.004). After thermocycling, there was no difference in the WOF values between testing in air or in water (p = 0.174–0.940).

3.2. Flexural strength and elastic modulus

Due to the interactions between the variables (partial eta-squared (η_p^2) = 0.057–0.294, p < 0.001–0.009), the results were split and analyzed separately.

3.2.1. Impact of the material on flexural strength and elastic modulus

Within the water-stored group tested in air-23 °C, VPR showed the highest FS, followed by DEN and FRE (p < 0.001–0.290) (Table 3,

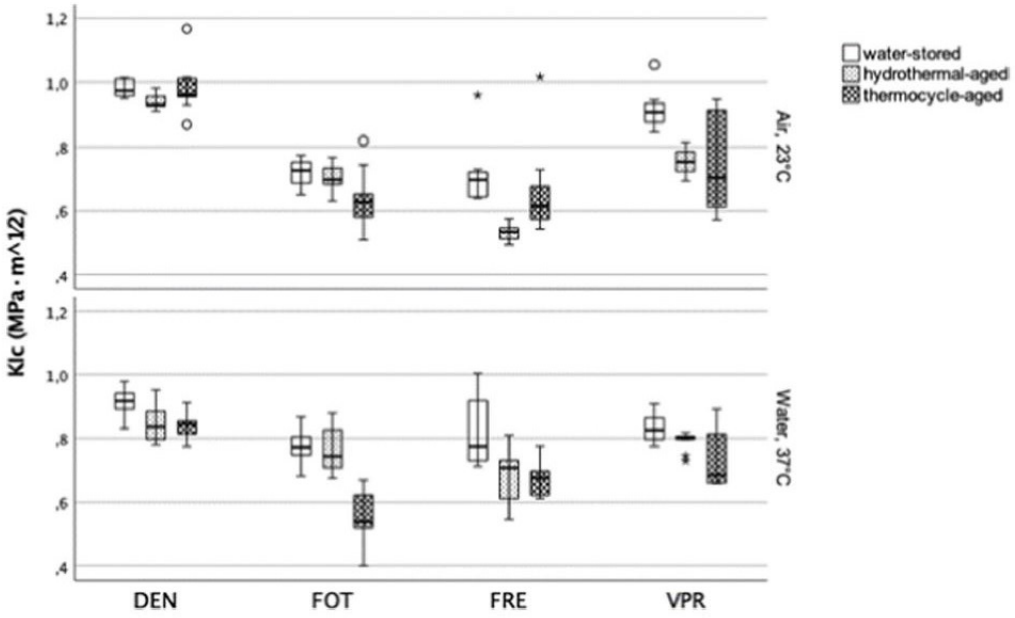

Fig. 6. Boxplots for the fracture toughness of each group.

Table 3
Descriptive statistics for FS (N/mm^2) and E (GPa) with mean, standard deviation (SD) and 95% confidence interval (CI); and Weibull modulus *m* with 95% CI.

		DEN		FOT		FRE		VPR	
		Mean ± SD	95% CI	Mean ± SD	95% CI	Mean ± SD	95% CI	Mean ± SD	95% CI
water-stored									
Air, 23 °C	FS	$98.3 \pm 9.5^{b,C,\beta}$	(90; 106)	$84.8 \pm 2.4^{a,C,\beta}$	(81; 88)	$104.2 \pm 8.5^{b,B,\alpha}$	(97; 109)	$112.1 \pm 6.6^{c,C,\beta}$	(106; 117)
	E	$3.14 \pm 0.11^{c,C,\beta}$	(3.05; 3.22)	$2.41 \pm 0.03^{a,C,\beta}$	(2.37; 2.43)	$3.11 \pm 0.08^{c,B,\beta}$	(3.04; 3.17)	$3.04 \pm 0.06^{b,C,\beta}$	(2.97; 3.08)
	m	$11.6^{a,B,\alpha}$	(5.9; 22.4)	$39.0^{b,B,\beta}$	(17.8; 84.9)	$14.6^{a,B,\alpha}$	(7.5; 28.1)	$20.1^{ab,B,\alpha}$	(10.4; 38.6)
Water, 37 °C	FS	$72.9 \pm 3.4^{b,B,\alpha}$	(69; 76)	$53.6 \pm 17.6^{a,A,\alpha}$	(30; 76)	$96.6 \pm 8.2^{c,B,\alpha}$	(89; 103)	$92.1 \pm 5.7^{c,C,\alpha}$	(87; 97)
	E	$2.40 \pm 0.12^{b,B,\alpha}$	(2.31; 2.49)	$2.06 \pm 0.56^{a,B,\alpha}$	(1.98; 2.14)	$2.70 \pm 0.11^{a,c,B,\alpha}$	(2.61; 2.79)	$2.70 \pm 0.13^{c,B,\alpha}$	(2.59; 2.80)
	m	$25.3^{c,B,\beta}$	(13.1; 48.6)	$3.1^{a,A,\alpha}$	(1.1; 7.9)	$13.0^{b,B,\alpha}$	(6.7; 25.0)	$18.5^{bc,C,\alpha}$	(9.5; 35.4)
hydrothermal-aged									
Air, 23 °C	FS	$74.6 \pm 20.0^{ab,A,\alpha}$	(59; 89)	$66.1 \pm 10.6^{b,A,\alpha}$	(56; 75)	$64.3 \pm 19.6^{b,A,\alpha}$	(49; 79)	$32.3 \pm 5.9^{a,A,\alpha}$	(27; 37)
	E	$2.66 \pm 0.13^{b,A,\beta}$	(2.55; 2.75)	$1.98 \pm 0.13^{a,A,\alpha}$	(1.87; 2.09)	$3.11 \pm 0.23^{a,c,B,\beta}$	(2.93; 3.27)	$2.61 \pm 0.17^{ab,A,\alpha}$	(2.47; 2.73)
	m	$3.8^{ab,A,\alpha}$	(1.8; 7.4)	$6.5^{b,A,\beta}$	(3.1; 12.9)	$3.3^{a,A,\alpha}$	(1.6; 6.4)	$6.9^{b,A,\beta}$	(3.4; 13.2)
Water, 37 °C	FS	$60.0 \pm 10.7^{aa,A,\alpha}$	(51; 68)	$50.2 \pm 23.6^{a,A,\alpha}$	(24; 75)	$75.2 \pm 23.2^{ab,A,\alpha}$	(57; 92)	$46.7 \pm 18.0^{a,A,\beta}$	(32; 60)
	E	$2.13 \pm 0.11^{b,A,\alpha}$	(2.03; 2.21)	$1.96 \pm 0.04^{a,A,\alpha}$	(1.91; 2.00)	$2.36 \pm 0.12^{c,A,\alpha}$	(2.26; 2.46)	$2.55 \pm 0.15^{d,A,\alpha}$	(2.43; 2.67)
	m	$5.8^{b,A,\alpha}$	(2.9; 11.2)	$1.8^{a,A,\alpha}$	(0.6; 4.3)	$2.8^{a,A,\alpha}$	(1.3; 5.4)	$2.8^{a,A,\alpha}$	(1.3; 5.5)
thermocycle-aged									
Air, 23 °C	FS	$91.5 \pm 7.5^{ab,B,\beta}$	(85; 97)	$74.4 \pm 13.7^{aa,B,\beta}$	(62; 86)	$96.5 \pm 19.2^{b,B,\beta}$	(81; 111)	$92.5 \pm 10.4^{ab,B,\beta}$	(83; 100)
	E	$2.99 \pm 0.09^{c,B,\beta}$	(2.92; 3.06)	$2.28 \pm 0.07^{a,B,\beta}$	(2.21; 2.34)	$2.95 \pm 0.10^{c,A,\beta}$	(2.86; 3.03)	$2.87 \pm 0.04^{b,B,\beta}$	(2.83; 2.91)
	m	$14.0^{b,B,\alpha}$	(7.2; 26.9)	$5.8^{a,A,\alpha}$	(2.7; 11.5)	$5.1^{a,A,\alpha}$	(2.5; 9.8)	$10.0^{ab,AB,\alpha}$	(5.1; 19.2)
Water, 37 °C	FS	$70.9 \pm 8.6^{ab,B,\alpha}$	(63; 77)	$63.1 \pm 1.6^{a,A,\alpha}$	(60; 65)	$86.6 \pm 11.4^{ac,A,\alpha}$	(77; 95)	$70.0 \pm 12.4^{ab,B,\alpha}$	(60; 79)
	E	$2.52 \pm 0.14^{b,B,\alpha}$	(2.41; 2.63)	$2.04 \pm 0.07^{a,AB,\alpha}$	(1.96; 2.10)	$2.75 \pm 0.08^{c,B,\alpha}$	(2.68; 2.81)	$2.53 \pm 0.11^{ab,A,\alpha}$	(2.44; 2.61)
	m	$9.3^{a,A,\alpha}$	(4.7; 17.9)	$45.3^{b,B,\beta}$	(20.7; 98.6)	$8.3^{a,B,\alpha}$	(4.2; 15.9)	$6.0^{a,B,\alpha}$	(3.0; 11.5)

^{a,b,c,d} indicate significant differences between materials within one aging level and one measurement environment.
^{A,B,C} indicate significant differences between aging levels within one material and one measurement environment.
$^{\alpha,\beta}$ indicate significant differences between measurement environments within one aging level and one material.
CI=Confidence Interval.
SD= Standard Deviation.
[a] Deviation from the normal distribution.

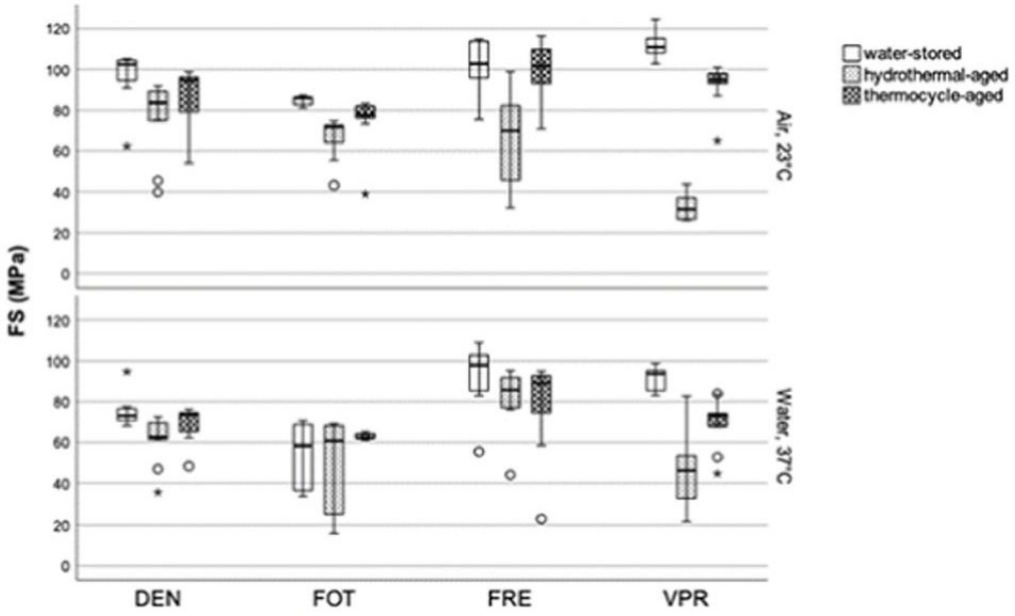

Fig. 7. Boxplots for the flexural strength of each group.

Fig. 7). DEN and FRE showed the highest E, followed by VPR ($p <$ 0,001–0.597). FOT showed higher *m* than DEN and FRE. When tested in water-37 °C, FRE and VPR showed the highest FS and E, followed by DEN ($p < 0.001$–0.257). DEN and VPR showed the highest *m*, followed by FRE and FOT. For both measurement environments, FOT showed the lowest FS and E values ($p < 0.001$–0.100).

Within hydrothermal-aged groups and specimens tested in air-23 °C, DEN, FOT and FRE showed higher FS than VPR ($p < 0.001$–0.683), while FRE showed the highest E followed by DEN/VPR ($p <$ 0.001–0.450). FOT and VPR showed higher *m* than FRE. When tested in water-37 °C, FRE showed higher FS than all other materials ($p = 0.013$–0.664) and VPR showed the highest E followed by FRE and DEN ($p < 0.001$–0.016). For the hydrothermal aged groups, FOT showed the lowest E values ($p <$ 0.001–0.450). DEN showed the highest *m*.

Within thermocycle-aged groups and specimens tested in air-23 °C, DEN, FRE and VPR showed higher FS and E than FOT (p = 0.001–0.597), with DEN presenting a higher *m* than FOT and FRE. When tested in water-37 °C, FRE showed the highest FS and E values, followed by DEN and VPR (p = 0.002–0.496). FOT showed the lowest FS and E (p = 0.006–0.040), while presenting the highest *m*.

DEN, FRE and VPR showed a fracture between the printing layers or, for most groups, a complex fracture into ≥3 parts (Table 4). In a frequency of 10.00–50.00, FOT presented a deformation, with its other specimens showing a fracture into 2 or more parts.

3.2.2. Impact of artificial aging on flexural strength and elastic modulus

For groups tested in air-23 °C, DEN, FOT and VPR showed the highest FS and E after water-storage, followed by thermocycling, while the hydrothermal-aged groups showed the lowest values (p < 0.001–0.041). For FRE, the highest FS values were reported after water-storage and thermocycling and the highest E after water-storage and hydrothermal aging (p < 0.001–0.597). FOT and FRE showed the highest *m* after water-storage. DEN and VPR showed the highest *m* after water-storage and thermocycling.

For groups tested in water-37 °C, DEN showed the highest FS and E after water-storge and thermocycling (p < 0.001–0.880). FRE presented the highest values after water-storage (p = 0.004–0.131). For VPR, the water-stored group showed the highest FS and E values, followed by the thermocycle-aged and then the hydrothermal-aged group, where there were no differences in E values between hydrothermal aging and thermocycling (p < 0.001–1.0). DEN showed the highest *m* after water-storage. FOT presented the highest *m* after thermocycling. FRE showed the highest values in the water-stored and thermocycle-aged groups. VPR showed the highest *m* after water-storage, followed by thermocycling and hydrothermal-aging.

While most groups (87.5%) showed a complex fracture after water storage, thermocycling led to an increased occurrence of fracture pattern (2). This trend was amplified by hydrothermal aging, with 29% of groups showing a fracture between the printing layers.

3.2.3. Impact of the measurement environment on flexural strength and elastic modulus

Water-stored DEN, FOT and VPR showed higher FS when examined in air-23 °C than in water-37 °C (p < 0.001–0.004). DEN presented higher *m* when measured in water-37 °C, while FOT showed higher *m* when examined in air-23 °C.

Hydrothermal-aged VPR presented higher FS (p = 0.041) when measured in water-37 °C. FOT and VPR showed higher *m* when tested in air-23 °C.

After thermocycling, all materials showed higher FS when examined in air-23 °C than in water-37 °C (p < 0.001–0.028). FOT presented higher *m* when examined in water-37 °C.

All groups showed higher E values when tested in air (p < 0.00100.004). Only FOT and hydrothermal aged VPR groups showed no difference in E between the measurement environments (p = 0.174–0.289).

When specimens were measured in water-37 °C, an increased occurrence of fracture pattern (2) (Fig. 5b) at the cost of fracture pattern (3) (Fig. 5c), viz. a decrease of fracture parts into solely two pieces, and a higher frequency of deformations (Fig. 5a) was observed.

Spearman's ρ showed a weak negative correlation between WOF and E (R = −0.193, p = 0.002) and a positive correlation between the other measured variables (R = 0.159–0.874, p=<0.001–0.009), with the exception of FS and WOF (R = −0.082, p = 0.111).

4. Discussion

The aim of this investigation was to examine the influence of artificial aging and the measurement environment on the mechanical properties of 3D-printed denture base resins. The tested hypotheses stating that neither the choice of denture base resin, artificial aging nor the measurement environment showed an impact on fracture toughness, work of fracture, flexural strength, elastic modulus or the Weibull moduli are rejected. With fracture toughness, flexural strength and elastic modulus showing a correlation, this assumption was accepted.

4.1. Material

Since all four additively manufactured denture base resins were printed using the same parameters, groups differed based on the materials' compositions and the employed post-processing methods. Since the exact composition is not disclosed by the manufacturer, it is difficult to attribute differences in the mechanical properties of the examined materials to their individual components. During the printing process, the curing of the liquid resin layer-by-layer can lead to an insufficient curing intensity in each added layer, which results in reduced chain

Table 4
Fracture type distribution [*(1)* deformation, *(2)* fracture between the printing layers resulting in two fracture pieces, *(3)* complex fracture into ≥3 parts] of the FS specimens (%) with 95% confidence interval (CI).

		DEN		FOT		FRE		VPR	
water-stored									
		n	95% CI	n	95% CI	n	95% CI	n	95% CI
Air, 23 °C	*(1)*	0	(0–31)	30	(5–66)	0	(0–31)	0	(0–31)
	(2)	0	(0–31)	0	(0–31)	0	(0–31)	0	(0–31)
	(3)	100	(68–100)	70	(33–94)	100	(68–100)	100	(68–100)
Water, 37 °C	*(1)*	0	(0–31)	50	(17–82)	0	(0–31)	0	(0–31)
	(2)	0	(0–31)	20	(1–56)	0	(0–31)	0	(0–31)
	(3)	100	(68–100)	30	(5–66)	100	(68–100)	100	(68–100)
hydrothermal-aged									
Air, 23 °C	*(1)*	0	(0–31)	10	(0–45)	0	(0–31)	0	(0–31)
	(2)	30	(5–66)	10	(0–45)	0	(0–31)	100	(68–100)
	(3)	70	(33–94)	80	(43–98)	100	(68–100)	0	(0–31)
Water, 37 °C	*(1)*	0	(0–31)	40	(11–74)	0	(0–31)	0	(0–31)
	(2)	100	(68–100)	20	(1–56)	20	(1–56)	90	(54–100)
	(3)	0	(0–31)	40	(11–74)	80	(43–98)	10	(0–45)
thermocycle-aged									
Air, 23 °C	*(1)*	0	(0–31)	10	(0–45)	0	(0–31)	0	(0–31)
	(2)	0	(0–31)	0	(0–31)	0	(0–31)	0	(0–31)
	(3)	100	(68–100)	90	(54–100)	100	(68–100)	100	(68–100)
Water, 37 °C	*(1)*	0	(0–31)	30	(5–66)	0	(0–31)	0	(0–31)
	(2)	100	(68–100)	20	(1–56)	0	(0–31)	20	(1–56)
	(3)	0	(0–31)	50	(17–82)	100	(68–100)	80	(43–98)

crosslinking (Kim et al., 2020). However, several investigations have shown that an efficient post-curing leads to adequate mechanical properties by increasing the degree of conversion, even after undergoing aging procedures (Kim et al., 2020; Monzón et al., 2017; Aati et al., 2022). The present investigation reporting high K_{IC} values for DEN and VPR and low values for FOT and FRE is in line with previous investigations, in which materials post-cured in an UV-Lightbox showed higher mechanical properties, e.g., E_{IT}, than materials post-cured under nitrogen atmosphere using flashlight polymerization (Otoflash) (Li et al., 2021b; Greil et al., 2023). The efficacy of the post-curing procedure is closely linked to the employed wavelengths of the polymerization devices. The photo initiator in all four materials is trimethylbenzoyl-diphenyl-phosphine oxide (TPO), which has an absorption peak at around 380 nm (Neumann et al., 2005; Schneider et al., 2012). This wavelength is covered by the radiation spectra of both polymerization devices used in this investigation. The continuous irradiation and extended post-curing duration of 30 min in the UV-Lightbox may increase the degree of conversion, which is reflected in higher mechanical properties (Li et al., 2021b). On the other side the wavelength peaks of the Otoflash (480 + 530 nm) are higher than the absorption spectrum of the photo initiator. The low values observed for FOT may be related to its post-curing process, where in contrast to the other materials, FOT was heated to 90 °C for 10 min after undergoing polymerization in the Otoflash. After production, FOT already showed signs of thermal aging such as superficial cracks and a flaking of the outer layer, that may be causal for this material's reduced mechanical properties. In addition to post-curing, the washing procedures after printing show an influence on the mechanical properties of the printed objects. A prolonged propanol washing has been reported to reduce the strength of 3D-printed specimens (Nowacki et al., 2021). With FOT undergoing the shortest washing, one may thus expect this material to show the highest mechanical properties. As this is not the case, the differences between the washing durations and the use of ethanol or isopropanol may be negligible in the present investigation. In addition, FOT was the only material that did not break during testing but presented a deformation of the specimens, an observation that is in line with the previously reported low elastic indentation modulus of this material (Greil et al., 2023). However, no material met the requirements for improved impact resistance given in the ISO standards (ISO, 20795–1, 2013). When comparing the four tested materials with regard to FS, DEN and FRE met the 60 MPa mark defined by the ISO norm even after undergoing hydrothermal and thermal aging, while FOT and VPR did not reach this threshold (ISO, 20795–1, 2013). Considering E, all groups except hydrothermal aged FOT (1.96 and 1.98 GPa), met the required 2 GPa mark. Nonetheless, none of the tested materials showed an improved impact resistance, with K_{IC} and WOF values being considerably lower (0.53–0.98 MPa $m^{1/2}$ min/31.2–130.6 J/m^2) than the required 1.9 MPa $m^{1/2}$ min/900 J/m^2. Previous investigations have already shown that 3D-printed acrylics have lower mechanical properties than most other denture base materials (Prpić et al., 2020; Perea-Lowery et al., 2021).

4.2. Artificial aging

Both hydrothermal- and thermocycle aging led to reduced mechanical properties. The examined materials were thus susceptible to artificial aging, a property which may impair the long-term stability of these materials in the oral cavity. Previous investigations have reported that water penetration into the resin matrix can lead to a softening of the material (Ferracane et al., 1998). The higher temperatures during aging may increase the ability of the resins to absorb water (Schoeffel et al., 2019). When water is absorbed in the resins polymer, the ester bond cleavage can lead to lower mechanical properties (Kwon et al., 2021). This hypothesis is supported by the fractographic analyses showing a fracture into less pieces following thermocycling and especially hydrothermal aging, indicating a less brittle behavior of the resin specimens. The intrusion of water may be reduced by optimized polishing protocols or a sealing of the surface by applying a glaze material, thus reducing imperfections on the surface of the specimens that may constitute fracture origins (Fig. 8). The fact that the hydrothermal aged groups (124 °C) showed lower FS and E values than observed after thermocycling (55 °C) led to the assumption, that the higher the temperature while aging, the higher the ability to absorb water. Future studies are warranted to examine if this behavior is caused by a dissolvement of the 3D-print resins caused by the increased temperature or connected to a leaching of the polymer or a possibly on-going post-polymerization. All materials showed the highest values for the FS Weibull modulus after water-storage and the lowest after hydrothermal aging, which suggests that not only the mechanical properties are reduced, but also that the distribution of the data increases.

4.3. Measurement environment

While there were no clear trends for K_{IC}, testing in water led to decreased FS and E values. When the specimens were tested in water, moisture may have been absorbed into the material through pre-existing holes, cracks and printing layers that are a result of the additive manufacturing process and may have been exacerbated by aging, which can decrease the mechanical properties of the objects (Prechtel et al., 2020). The increased occurrence of facture pattern (2) at the cost of fracture pattern (3) and the higher frequency of deformations as well as the lower E values in almost all groups indicates that a measurement in water results in a more elastic behavior of the resin specimens during testing. The high FS values measured in air may thus distort predictions for the clinical situation, which is defined by its moist environment at body temperature. Even if all examined materials would meet the ISO requirements for FS (65 MPa) and E (2 GPa) (ISO, 20795–1, 2013), the clinical conditions in the patient are thus not adequately reproduced during the measurements. This is particularly notable since previous studies have already shown that 3D printed denture resins have a higher water absorption and in consequence lower strength values (Greil et al., 2023; Perea-Lowery et al., 2021). To allow valid estimates of a material's performance in situ, in-vitro measurements should thus be performed in water at 37 °C.

The fact that 28.3% of FOT FS test specimens did not break during the measurements but were deformed until maximum displacement was reached calls into question the measurement methods specified in the ISO standards. A previous study has already criticized the rationale of the cut-off values in the ISO norm (Steinmassl et al., 2018), underlining

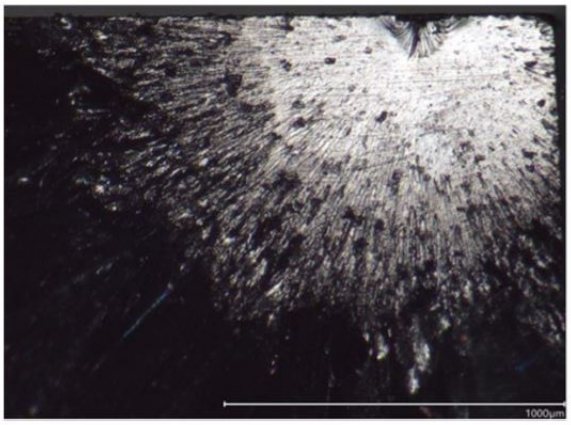

Fig. 8. View onto the lateral fracture surface. The fracture originated from a surface flaw (red arrow) on the tensile side. The blue arrows indicate the direction of crack propagation.

the need for a revised definition of the measurement set-ups and required threshold values that incorporate the elastic properties of 3D-print resins used for the additive manufacturing of denture base materials. For ceramic test specimens, a notch length of 1.5x the cut radius has been propagated (Fett, 1995). The inclusion of the notch radius in the ISO norm would standardize measurements further.

In a previous investigation, the water sorption, water solubility, degree of conversion, elastic indentation modulus, edge chipping resistance and flexural strength of the same four 3D-printed denture base resins were determined and compared with a milled and a conventionally polymerized control group, reporting that only FOT and FRE surpassed the threshold values defined by the ISO norm. In light of the present findings, where FRE showed similar K_{IC} and superior FS and E values in comparison with FOT, FRE may thus represent the 3D-print denture base resin material of choice.

Limitation of this in vitro investigation include the limited number of examined materials and information about the exact composition of the tested materials. Further research investigating other printing geometries, various material compositions and different post-curing methods are recommended.

5. Conclusions

Within the limitations of this study, the following conclusions can be drawn:

1. DEN, FRE and VPR met the 60 MPa mark defined by the ISO norm for FS, while none of the tested materials reached the requirements for improved impact resistance.
2. Hydrothermal-aging and thermocycling led to reduced mechanical properties and number of FS fracture pieces.
3. With measurements in air-23°C resulting in higher FS values and a more brittle fracture behavior than observed for measurements in water-37°C, the measurement environment during future in vitro investigations should be adapted to the clinical situation to allow valid predictions on the mechanical behavior of the examined materials, e.g., denture base resins, when in situ.

CRediT authorship contribution statement

Veronika Geiger: Writing – original draft, Methodology, Investigation, Data curation. **Felicitas Mayinger:** Writing – review & editing, Writing – original draft, Supervision, Methodology. **Moritz Hoffmann:** Writing – review & editing, Project administration. **Marcel Reymus:** Writing – review & editing, Project administration. **Bogna Stawarczyk:** Writing – review & editing, Supervision, Project administration, Methodology.

Declaration of competing interest

The authors declare that they have no known competing financial interests or personal relationships that could have appeared to influence the work reported in this paper.

Data availability

Data will be made available on request.

Acknowledgements

The authors thank DETAX, Dreve ProDiMed, NextDent and VOCO for supporting this investigation.

This research did not receive any specific grant from funding agencies in the public, commercial, or not-for-profit sectors.

References

Aati, S., Akram, Z., Shrestha, B., Patel, J., Shih, B., Shearston, K., et al., 2022. Effect of post-curing light exposure time on the physico-mechanical properties and cytotoxicity of 3D-printed denture base material. Dent. Mater. 38, 57–67. https://doi.org/10.1016/j.dental.2021.10.011.

Alharbi, N., Wismeijer, D., Osman, R.B., 2017. Additive manufacturing techniques in prosthodontics: where do we currently stand? A critical review. Int. J. Prosthodont. (IJP) 30, 474–484. https://doi.org/10.11607/ijp.5079.

Bilgin, M.S., Baytaroğlu, E.N., Erdem, A., Dilber, E., 2016. A review of computer-aided design/computer-aided manufacture techniques for removable denture fabrication. Eur. J. Dermatol. 10, 286–291. https://doi.org/10.4103/1305-7456.178304.

Chevalier, J., 2006. What future for zirconia as a biomaterial? Biomaterials 27, 535–543. https://doi.org/10.1016/j.biomaterials.2005.07.034.

Duret, F., Preston, J.D., 1991. CAD/CAM imaging in dentistry. Curr. Opin. Dent. 1, 150–154.

Ferracane, J.L., Berge, H.X., Condon, J.R., 1998. In vitro aging of dental composites in water?Effect of degree of conversion, filler volume, and filler/matrix coupling. J. Biomed. Mater. Res. 42, 465–472. https://doi.org/10.1002/(SICI)1097-4636(19981205)42:3<465::AID-JBM17>3.0.CO;2-F.

Fett, T., 1995. Notch effects in determination of fracture toughness and compliance. Int. J. Fract. 72, R27–R30. https://doi.org/10.1007/BF00042831.

Gale, M., Darvell, B., 1999. Thermal cycling procedures for laboratory testing of dental restorations. J. Dent. 27, 89–99. https://doi.org/10.1016/s0300-5712(98)00037-2.

Greil, V., Mayinger, F., Reymus, M., Stawarczyk, B., 2023. Water sorption, water solubility, degree of conversion, elastic indentation modulus, edge chipping resistance and flexural strength of 3D-printed denture base resins. J. Mech. Behav. Biomed. Mater. 137, 105565 https://doi.org/10.1016/j.jmbbm.2022.105565.

ISO 20795–1, 2013. Dentistry – Base Polymers. Part 1: Denture Base Polymers, second ed. International Organization for Standardization, Geneva, Switzerland.

Kim, D., Shim, J.-S., Lee, D., Shin, S.-H., Nam, N.-E., Park, K.-H., et al., 2020. Effects of post-curing time on the mechanical and color properties of three-dimensional printed crown and bridge materials. Polymers 12. https://doi.org/10.3390/polym12112762. Basel.

Kwon, J.-S., Kim, J.-Y., Mangal, U., Seo, J.-Y., Lee, M.-J., Jin, J., et al., 2021. Durable oral biofilm resistance of 3D-printed dental base polymers containing zwitterionic materials. Int. J. Mol. Sci. 22 https://doi.org/10.3390/ijms22010417.

Li, P., Krämer-Fernandez, P., Klink, A., Xu, Y., Spintzyk, S., 2021a. Repairability of a 3D printed denture base polymer: effects of surface treatment and artificial aging on the shear bond strength. J. Mech. Behav. Biomed. Mater. 114, 104227 https://doi.org/10.1016/j.jmbbm.2020.104227.

Li, P., Lambart, A.-L., Stawarczyk, B., Reymus, M., Spintzyk, S., 2021b. Postpolymerization of a 3D-printed denture base polymer: impact of post-curing methods on surface characteristics, flexural strength, and cytotoxicity. J. Dent. 115, 103856 https://doi.org/10.1016/j.jdent.2021.103856.

Miyazaki, T., Hotta, Y., Kunii, J., Kuriyama, S., Tamaki, Y., 2009. A review of dental CAD/CAM: current status and future perspectives from 20 years of experience. Dent. Mater. J. 28, 44–56. https://doi.org/10.4012/dmj.28.44.

Monzón, M., Ortega, Z., Hernández, A., Paz, R., Ortega, F., 2017. Anisotropy of photopolymer parts made by digital light processing. Materials 10. https://doi.org/10.3390/ma10010064. Basel.

Neumann, M.G., Miranda, W.G., Schmitt, C.C., Rueggeberg, F.A., Correa, I.C., 2005. Molar extinction coefficients and the photon absorption efficiency of dental photoinitiators and light curing units. J. Dent. 33, 525–532. https://doi.org/10.1016/j.jdent.2004.11.013.

Nowacki, B., Kowol, P., Kozioł, M., Olesik, P., Wieczorek, J., Wacławiak, K., 2021. Effect of post-process curing and washing time on mechanical properties of mSLA printouts. Materials 14. https://doi.org/10.3390/ma14174856.

Oberoi, G., Nitsch, S., Edelmayer, M., Janjić, K., Müller, A.S., Agis, H., 2018. 3D printing-encompassing the facets of dentistry. Front. Bioeng. Biotechnol. 6, 172. https://doi.org/10.3389/fbioe.2018.00172.

Oliveira Limírio Jpj de, Gomes, JMdL., Alves Rezende, M.C.R., Lemos, C.A.A., Del Rosa, C.D.R.D., Pellizzer, E.P., 2021. Mechanical properties of polymethyl methacrylate as a denture base: conventional versus CAD-CAM resin - a systematic review and meta-analysis of in vitro studies. J. Prosthet. Dent. https://doi.org/10.1016/j.prosdent.2021.03.018.

Perea-Lowery, L., Gibreel, M., Vallittu, P.K., Lassila, L.V., 2021. 3D-Printed vs. Heat-polymerizing and autopolymerizing denture base acrylic resins. Materials 14. https://doi.org/10.3390/ma14195781.

Prechtel, A., Reymus, M., Edelhoff, D., Hickel, R., Stawarczyk, B., 2020. Comparison of various 3D printed and milled PAEK materials: effect of printing direction and artificial aging on Martens parameters. Dent. Mater. 36, 197–209. https://doi.org/10.1016/j.dental.2019.11.017.

Prpić, V., Schauperl, Z., Ćatić, A., Dulčić, N., Čimić, S., 2020. Comparison of mechanical properties of 3D-printed, CAD/CAM, and conventional denture base materials. J. Prosthodont. 29, 524–528. https://doi.org/10.1111/jopr.13175.

Reymus, M., Fabritius, R., Keßler, A., Hickel, R., Edelhoff, D., Stawarczyk, B., 2020. Fracture load of 3D-printed fixed dental prostheses compared with milled and conventionally fabricated ones: the impact of resin material, build direction, post-curing, and artificial aging-an in vitro study. Clin. Oral Invest. 24, 701–710. https://doi.org/10.1007/s00784-019-02952-7.

Roos, M., Stawarczyk, B., 2012. Evaluation of bond strength of resin cements using different general-purpose statistical software packages for two-parameter Weibull statistics. Dent. Mater. 28, e76–e88. https://doi.org/10.1016/j.dental.2012.04.013.

Schneider, L.F.J., Cavalcante, L.M., Prahl, S.A., Pfeifer, C.S., Ferracane, J.L., 2012. Curing efficiency of dental resin composites formulated with camphorquinone or

trimethylbenzoyl-diphenyl-phosphine oxide. Dent. Mater. 28, 392–397. https://doi.org/10.1016/j.dental.2011.11.014.
Schoeffel, A.C., Bagio, P., Sakima, V.T., Soares, S., Neppelenbroek, K.H., Urban, V.M., 2019. Knoop microhardness of conventional and microwaved denture base acrylic resins. Indian J. Dent. Res. 30, 927–932. https://doi.org/10.4103/ijdr.IJDR_436_17.
Steinmassl, O., Offermanns, V., Stöckl, W., Dumfahrt, H., Grunert, I., Steinmassl, P.-A., 2018. In vitro analysis of the fracture resistance of CAD/CAM denture base resins. Materials 11. https://doi.org/10.3390/ma11030401. Basel.
Sun, J., Zhang, F.-Q., 2012. The application of rapid prototyping in prosthodontics. J. Prosthodont. 21, 641–644. https://doi.org/10.1111/j.1532-849X.2012.00888.x.
van Noort, R., 2012. The future of dental devices is digital. Dent. Mater. 28, 3–12. https://doi.org/10.1016/j.dental.2011.10.014.
Webb, P.A., 2000. A review of rapid prototyping (RP) techniques in the medical and biomedical sector. J. Med. Eng. Technol. 24, 149–153. https://doi.org/10.1080/03091900050163427.

Literaturverzeichnis

[1] Dawood A, Marti Marti B, Sauret-Jackson V, Darwood A. 3D printing in dentistry. Br Dent J 2015;219:521–9.

[2] Duret F, Preston JD. CAD/CAM imaging in dentistry. Curr Opin Dent 1991;1:150–4.

[3] Oliveira Limírio JPJ de, Gomes JMdL, Alves Rezende MCR, Lemos CAA, Del Rosa CDRD, Pellizzer EP. Mechanical properties of polymethyl methacrylate as a denture base: Conventional versus CAD-CAM resin - A systematic review and meta-analysis of in vitro studies. J Prosthet Dent 2021.

[4] Strub JR, Rekow ED, Witkowski S. Computer-aided design and fabrication of dental restorations: current systems and future possibilities. J Am Dent Assoc 2006;137:1289–96.

[5] Alharbi N, Wismeijer D, Osman RB. Additive Manufacturing Techniques in Prosthodontics: Where Do We Currently Stand? A Critical Review. Int J Prosthodont 2017;30:474–84.

[6] Aati S, Akram Z, Shrestha B, Patel J, Shih B, Shearston K et al. Effect of post-curing light exposure time on the physico-mechanical properties and cytotoxicity of 3D-printed denture base material. Dent Mater 2022;38:57–67.

[7] Bilgin MS, Baytaroğlu EN, Erdem A, Dilber E. A review of computer-aided design/computer-aided manufacture techniques for removable denture fabrication. Eur J Dent 2016;10:286–91.

[8] Kessler A, Hickel R, Reymus M. 3D Printing in Dentistry-State of the Art. Oper Dent 2020;45:30–40.

[9] Tian Y, Chen C, Xu X, Wang J, Hou X, Li K et al. A Review of 3D Printing in Dentistry: Technologies, Affecting Factors, and Applications. Scanning 2021;2021:9950131.

[10] Whitley D, Eidson RS, Rudek I, Bencharit S. In-office fabrication of dental implant surgical guides using desktop stereolithographic printing and implant treatment planning software: A clinical report. J Prosthet Dent 2017;118:256–63.

[11] Miyazaki T, Hotta Y, Kunii J, Kuriyama S, Tamaki Y. A review of dental CAD/CAM: current status and future perspectives from 20 years of experience. Dent Mater J 2009;28:44-56.

[12] Webb PA. A review of rapid prototyping (RP) techniques in the medical and biomedical sector. J Med Eng Technol 2000;24:149–53.

[13] Sun J, Zhang F-Q. The application of rapid prototyping in prosthodontics. Journal of prosthodontics : official journal of the American College of Prosthodontists 2012;21:641–4.

[14] Zafar MS. Prosthodontic Applications of Polymethyl Methacrylate (PMMA): An Update. Polymers (Basel) 2020;12.

[15] Gad MM, Alshehri SZ, Alhamid SA, Albarrak A, Khan SQ, Alshahrani FA et al. Water Sorption, Solubility, and Translucency of 3D-Printed Denture Base Resins. Dent J (Basel) 2022;10.

[16] Perea-Lowery L, Gibreel M, Vallittu PK, Lassila LV. 3D-Printed vs. Heat-Polymerizing and Autopolymerizing Denture Base Acrylic Resins. Materials (Basel) 2021;14.

[17] Bartoloni JA, Murchison DF, Wofford DT, Sarkar NK. Degree of conversion in denture base materials for varied polymerization techniques. J Oral Rehabil 2000;27:488–93.

[18] Alhareb AO, Akil HM, Ahmad ZA. Impact strength, fracture toughness and hardness improvement of PMMA denture base through addition of nitrile rubber/ceramic fillers. The Saudi Journal for Dental Research 2017;8:26–34.

[19] Gale M, Darvell B. Thermal cycling procedures for laboratory testing of dental restorations. J Dent 1999;27:89–99.

[20] Li P, Krämer-Fernandez P, Klink A, Xu Y, Spintzyk S. Repairability of a 3D printed denture base polymer: Effects of surface treatment and artificial aging on the shear bond strength. J Mech Behav Biomed Mater 2021;114:104227.

[21] DIN EN ISO 20795-1; 2013. Dentistry – Base polymers. Part 1: Denture base polymers. International Organization for Standardization; 2nd ed. Geneva, Switzerland.

[22] Kim D, Shim J-S, Lee D, Shin S-H, Nam N-E, Park K-H et al. Effects of Post-Curing Time on the Mechanical and Color Properties of Three-Dimensional Printed Crown and Bridge Materials. Polymers (Basel) 2020;12.

[23] Neumann MG, Miranda WG, Schmitt CC, Rueggeberg FA, Correa IC. Molar extinction coefficients and the photon absorption efficiency of dental photoinitiators and light curing units. J Dent 2005;33:525–32.

[24] Schneider LFJ, Cavalcante LM, Prahl SA, Pfeifer CS, Ferracane JL. Curing efficiency of dental resin composites formulated with camphorquinone or trimethylbenzoyl-diphenyl-phosphine oxide. Dent Mater 2012;28:392–7.

[25] Ferracane JL, Berge HX, Condon JR. In vitro aging of dental composites in water?Effect of degree of conversion, filler volume, and filler/matrix coupling. J. Biomed. Mater. Res. 1998;42:465–72.

[26] Egilmez F, Ergun G, Cekic-Nagas I, Vallittu PK, Lassila LVJ. Does artificial aging affect mechanical properties of CAD/CAM composite materials. J Prosthodont Res 2018;62:65–74.

[27] Prechtel A, Reymus M, Edelhoff D, Hickel R, Stawarczyk B. Comparison of various 3D printed and milled PAEK materials: Effect of printing direction and artificial aging on Martens parameters. Dent Mater 2020;36:197–209.

[28] Steinmassl O, Offermanns V, Stöckl W, Dumfahrt H, Grunert I, Steinmassl P-A. In Vitro Analysis of the Fracture Resistance of CAD/CAM Denture Base Resins. Materials (Basel) 2018;11.

Danksagung

An dieser Stelle möchte ich meinen besonderen Dank allen Personen aussprechen, die meine Dissertation begleitet und mich wissenschaftlich, fachlich und emotional unterstützt haben.

Mein Dank gilt zunächst Frau Prof. Bogna Stawarczyk für die Betreuung dieser Arbeit sowie für ihre unermüdliche Motivation und Ideengebung. Ihre Expertise und Engagement haben die Durchführung dieser Arbeit erst möglich gemacht.

Ein besonderer Dank geht an Frau PD Dr. med. dent. Felicitas Mayinger, sowie insbesondere an Herrn PD Dr. med. dent. Marcel Reymus und Herrn Moritz Hoffmann, M.Sc. die mich mit ihrer Erfahrung und konstruktiven Feedbacks bei der Durchführung der Untersuchungen immer unterstützt haben.

Ich bedanke mich bei allen Mitarbeitern und Doktoranden der Werkstoffkunde der Poliklinik für Zahnärztliche Prothetik der LMU München für die schöne Zeit und die kollegiale Zusammenarbeit.

Des Weiteren möchte ich mich bei den Firmen DETAX, Dreve ProDiMed, NextDent und VOCO für die Bereitstellung der Materialien und die technische Unterstützung bei der Prüfkörperherstellung bedanken.

Ich bedanke mich bei meiner Familie, meinen Eltern Barbara und Alexander Greil und meiner Schwester Magdalena Greil, für ihre unendliche Unterstützung und bedingungslose Liebe. Sie haben mir meinen bisherigen Lebensweg ermöglicht, weshalb ich ihnen diese Arbeit widme.

Abschließend möchte ich meinem Mann Maximilian Geiger aus tiefsten Herzen danken. Er war stets an meiner Seite und hat mich in dieser anspruchsvollen Zeit mit viel Verständnis und Motivation begleitet.